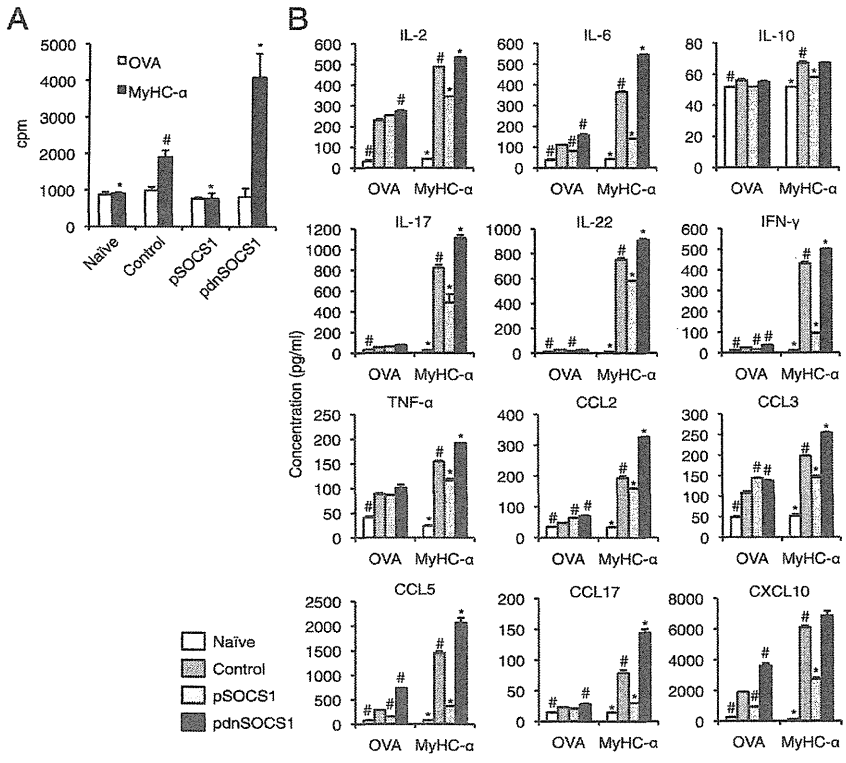

FIGURE 4. Impaired expansion of heart-specific $CD4^+$ T cells in pSOCS1-treated mice. (**A**) Splenocytes were isolated from naive and EAM mice treated with pSOCS1, pdnSOCS1, or control plasmid on day 14 and restimulated in vitro with MyHC-α or OVA peptide for 72 h. Proliferation was assessed by measurement of $[^3H]$thymidine incorporation. Data represent means ± SEM of triplicates from one of three independent experiments. (**B**) Cytokines and chemokines in the culture supernatants of splenocytes were measured by ELISA after 48 h of restimulation with MyHC-α or OVA peptide. Data are expressed as mean ± SEM from triplicate culture wells. Results of one of two representative experiments are shown. $^*p < 0.05$ compared with MyHC-α–stimulated control, $^\#p < 0.05$ compared with OVA-stimulated control.

delivery inhibits the activation of myosin-specific $CD4^+$ T cells and strongly suggest that impaired $CD4^+$ Th cell function prevents EAM development in pSOCS1-injected mice after immunization with cardiac self-Ag.

To evaluate whether pSOCS1 administration affects Ag-specific $CD4^+$ T cell function in other models, we injected plasmid DNA into an autoimmune gastritis model and an OVA-immunized model. In the autoimmune gastritis model, gastric-Ag–specific production of IL-2, IL-6, IL-13, IL-17, IL-22, IFN-γ, TNF-α, CCL2, CCL5, CCL17, and CXCL10 by $CD4^+$ T cells was decreased in pSOCS1-administered mice but increased in pdnSOCS1-administered mice (Supplemental Fig. 2). Lower amounts of cytokines (including IL-2, IL-6, IL-13, IFN-γ, TNF-α, CCL2, CCL3, CCL5, CCL17, and CXCL10) were also produced in $CD4^+$ T cells from pSOCS1-injected OVA-immunized mice (Supplemental Fig. 3). These results suggest that pSOCS1 administration may suppress Ag-specific $CD4^+$ T cell activation in various autoimmune diseases and foreign body infections.

SOCS1 DNA administration inhibits the production of proinflammatory cytokines and $CD4^+$ T cell differentiation in the heart

We also examined whether SOCS1 DNA administration has an effect on cytokine and chemokine milieu in the heart. On day 14 after MyHC-α immunization, heart homogenates from pSOCS1-injected mice had significantly decreased amounts of proinflammatory cytokines, including IL-1β and IL-6, and of myelotropic chemokines, including CCL5, CXCL1, and CXCL10 (Fig. 5A). In contrast, hearts from mice injected with pdnSOCS1 showed greatly increased amounts of proinflammatory cytokines and chemokines (Fig. 5A). SOCS1 protein has been shown to regulate T cell differentiation (17, 18). To determine the differentiation of $CD4^+$ T cells during EAM, we examined the heart-infiltrating $CD4^+$ T cell populations by FACS analysis. Activated $CD4^+$ T cells ($CD4^+CD40L^+$) and effector memory $CD4^+$ T cells ($CD44^+CD62L^-$) were reduced in the pSOCS1-injected mice (Fig. 5B). Thus, protection from EAM in pSOCS1-administered mice is associated with abrogation of proinflammatory cytokines, chemokines, and $CD4^+$ T cell differentiation in the heart.

SOCS1 DNA injection does not have a direct suppressive effect on $CD4^+$ T cell activation

To gain new insights into the mechanism of protection from myocarditis, we investigated whether pSOCS1 therapy directly affects $CD4^+$ T cell activation. Naive T cells ($CD4^+CD62L^+$ cells) were isolated from non-EAM mice injected with pSOCS1, pdnSOCS1, or control plasmid, and their primary responses to various stimuli were compared (Fig. 6A). As shown in Fig. 6B, there were no differences in IFN-γ–induced STAT1 activation among these $CD4^+$ T cells. There were also no differences in primary responses to stimulation with anti-CD3ε, anti-CD3ε/anti-CD28, PMA/ionomycin, or Con A presented by mitomycin C-treated wild-type DCs among pSOCS1-, pdnSOCS1-, and control plasmid-treated $CD4^+$ T cells (Fig. 6C). Chong et al. (30) demonstrated that SOCS1-deficient T cells produced substantially greater levels of IFN-γ in response to IL-2 or IL-12. From these findings, we assessed the production of IFN-γ from $CD4^+$ T cells by using the same experiments. In the culture supernatants of

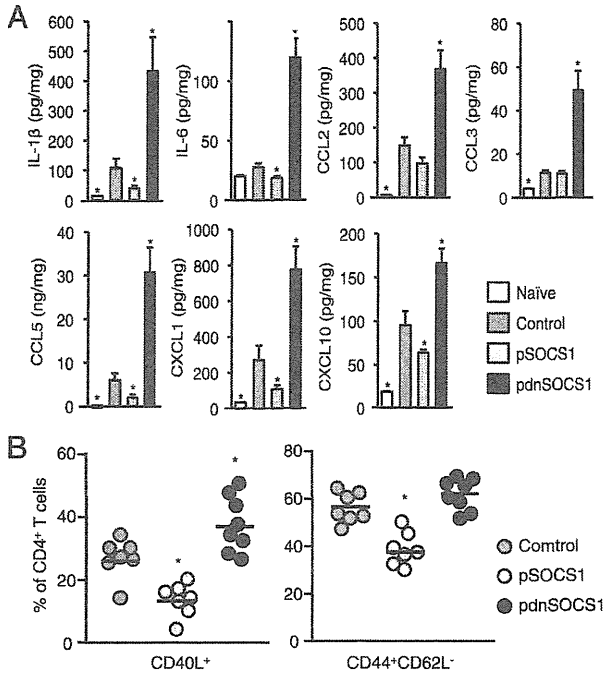

FIGURE 5. Cytokine and chemokine responses and $CD4^+$ T cell differentiation in the heart. (**A**) Myocardial tissues were homogenated and processed by ELISA to detect cytokines and chemokines on day 14. Bar graphs show group means ± SEM of 8–16 mice/group. Results of one of three representative experiments are shown. (**B**) Heart-infiltrating cells were isolated from EAM mice treated with indicated plasmid DNA. Cells were stained for CD4, CD40L, CD44, and CD62L. CD44 and CD62L expression are based on gates set from total $CD4^+$ T cells. Bar graphs show group means ± SEM of 5–9 mice/group. Data are representative of two independent experiments. $*p < 0.05$ compared with control.

$CD4^+$ T cells stimulated with IL-2 or IL-12, there were also no differences in IFN-γ production (Fig. 6D). These results indicate that in vivo administration of pSOCS1 does not directly affect $CD4^+$ T cell activation.

In vivo SOCS1 DNA administration inhibits DC function

Although $CD4^+$ T cell differentiation was inhibited in pSOCS1-treated mice (Fig. 5B), our results suggested that in vivo *Socs1* gene administration has no direct effect on $CD4^+$ T cell activation (Fig. 6). We therefore investigated whether in vivo pSOCS1 administration inhibits the function of Ag-presenting DCs by stimulation through the TLR pathway. DCs from mice administered pSOCS1, pdnSOCS1, or control plasmid were stimulated with LPS for 24 h (Fig. 7A). STAT1 phosphorylation was attenuated in DCs from pSOCS1-injected mice and enhanced in DCs from pdnSOCS1-injected mice (Fig. 7B). The production of proinflammatory cytokines, including IL-6, TNF-α, and IFN-γ, was inhibited in DCs from pSOCS1-injected mice and enhanced in DCs from pdnSOCS1-injected mice (Fig. 7C). These results indicate that in vivo administration of *Socs1* affects DC function. In the current study, the cardiac-Ag–specific proliferative response and cytokine production of $CD4^+$ T cells were inhibited in pSOCS1-injected EAM mice (Fig. 4). We next assessed the functional capability of DCs to prime and expand autoreactive $CD4^+$ T cells from mice injected with each plasmid as a measure of Ag-specific proliferative responses of $CD4^+$ T cells from MyHC-α–immunized mice. Myosin-specific $CD4^+$ T cells were cocultured with MyHC-α–pulsed DCs from pSOCS1-, pdnSOCS1-, and control plasmid-treated mice (Fig. 7D). Interestingly, the proliferative responses of $CD4^+$ T cells cocultured with DCs from pSOCS1-treated mice were much weaker than those of cells cultured with DCs from control plasmid-treated mice, and these proliferative responses of $CD4^+$ T cells were enhanced by coculturing with DCs from pdnSOCS1-administered mice (Fig. 7E). These results suggest that in vivo gene delivery of *Socs1* suppresses the functional capability of DCs to prime and expand autoreactive $CD4^+$ T cells.

SOCS1 DNA administration inhibits the development of myocarditis induced by cardiac myosin peptide-loaded BMDC transfer but not by $CD4^+$ T cell transfer

Functionally interposed SOCS1 is induced in various cell populations, including leukocytes, vascular cells, and cardiomyocytes (18, 31, 32). A mouse model of EAM was established by cell transfer using peptide-pulsed DCs or cardiac epitope-specific $CD4^+$ T cells (7, 14). The effects of pSOCS1 administration in mice transferred with $CD4^+$ T cells from mice with EAM were assessed. pSOCS1, pdnSOCS1, or control plasmid was injected into mice transferred with cardiac myosin-specific $CD4^+$ T cells (Fig. 8A). All mice transferred with $CD4^+$ T cells developed myocarditis, and no therapeutic effects were seen in pSOCS1-injected mice (Fig. 8B–D). Furthermore, pdnSOCS1 administration showed no adverse effect on the status of myocarditis induced by $CD4^+$ T cell transfer (Fig. 8B–D). These findings suggest that systemic injection of pSOCS1 is not effective for inhibition of autoreactive $CD4^+$ T cell activation and recruitment to the heart during myocarditis development. Next, we administered pSOCS1, pdnSOCS1, or control plasmid into mice transferred with MyHC-α–loaded BMDCs (Fig. 8E). Interestingly, pSOCS1 injection inhibited the development of myocarditis after MyHC-α–loaded BMDC transfer, and myocarditis deteriorated after administration of pdnSOCS1 (Fig. 8F–H). These results indicate that the therapeutic effects of SOCS1 DNA administration on EAM contribute to professional APCs such as DCs and also provide evidence for the potential utility of SOCS1 DNA inoculation as an approach to gene therapy for myocarditis.

Discussion

There have been no effective fundamental therapies for acute myocarditis; therefore, supportive care for LV dysfunction is the first line of treatment. Because patients generally present days to weeks after the initial viral infection, antiviral therapy has limited applicability in patients with acute viral myocarditis. The long-term sequelae of viral myocarditis appear to be related to abnormal cellular and humoral immunity; therefore, many clinicians believe that immunosuppression is beneficial for myocarditis treatment (2). In this study, we showed that administration of SOCS1 DNA is effective for inhibiting the development of EAM in BALB/c mice, suggesting a novel immunotherapy for myocarditis. To our knowledge, this is the first report showing that gene delivery of *Socs1* prevents autoimmune disease.

Animal models have greatly advanced our knowledge of the pathogenesis of myocarditis and inflammatory cardiomyopathy. Infection of BALB/c mice with either Coxsackievirus or murine CMV results in the development of acute myocarditis from days 7–14 postinfection that is characterized by myocyte damage due to viral cytotoxicity, and the infectious virus cannot be detected past day 14 of the infection (7). After elimination of viruses, mice showed autoimmune myocarditis, which is associated with mononuclear infiltration of the myocardium and production of autoantibodies to cardiac myosin (7), similar to the pathogenesis of autoimmune myocarditis in humans (3, 4, 33). These autoim-

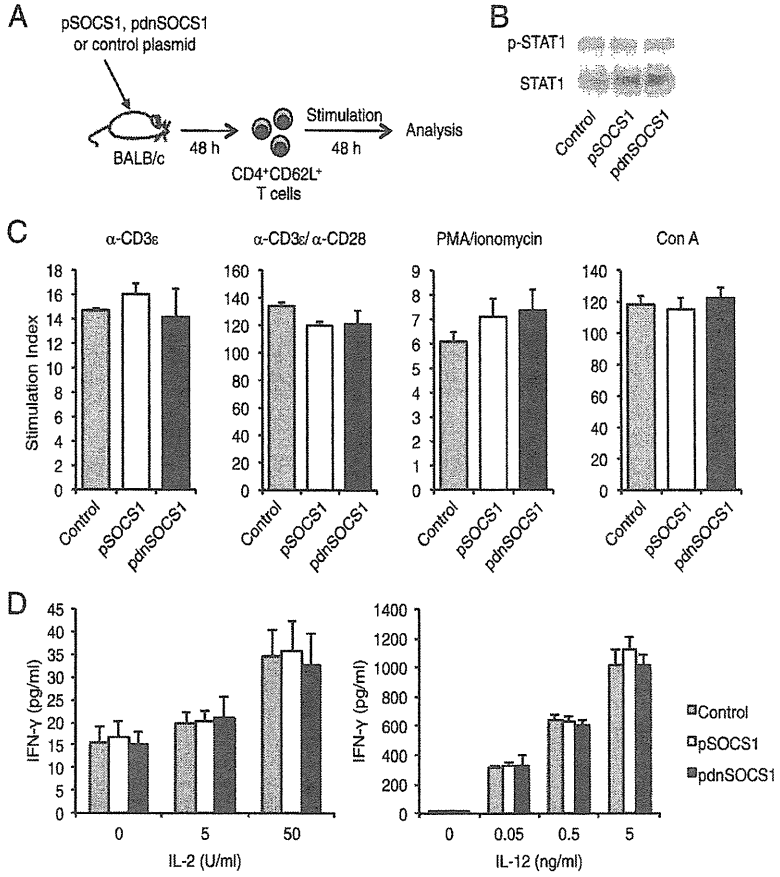

FIGURE 6. Primary responses of $CD4^+$ T cells from pSOCS1-, pdnSOCS1-, and control plasmid-treated mice. (**A**) $CD4^+CD62L^+$ T cells from mice injected with pSOCS1, pdnSOCS1, or control plasmid were stimulated with IFN-γ, anti-CD3ε, anti-CD3ε, anti-CD28, PMA/ionomycin, and Con A in the presence of wild-type DCs, IL-2, or IL-12. (**B**) STAT1 phosphorylation of $CD4^+$ T cells after IFN-γ treatment (10 ng/ml) was assessed by Western blotting. (**C**) T cell proliferation was measured after 48 h of culture. (**D**) IFN-γ in the culture supernatants was measured by ELISA. Values are expressed as means ± SEM of triplicate culture wells. Results of one of at least two representative experiments are shown.

mune responses are thought to be elicited by two mechanisms. One is molecular mimicry: responses to microbial Ags could result in the activation of T cells that are cross-reactive with self-Ags. Another possibility is bystander activation of autoreactive cells. APCs that have become activated in the inflammatory milieu of a pathogenic infection can stimulate the activation and proliferation of autoreactive T or B cells in a process known as bystander activation (reviewed in Ref. 34). Thus, immune responses to myocytes involving various innate and adaptive immune pathways were recognized during myocarditis development. The cardiac myosin peptide-immunized mouse EAM model reflects human autoimmune myocarditis and heart failure after elimination of infectious pathogens.

Recent studies have indicated that various microbes use the host's SOCS proteins for manipulating cytokine receptor signaling as one of the strategies to evade immune responses (35, 36). Coxsackievirus usually infects cardiomyocytes and induces the expression of SOCS1 and SOCS3 in cardiomyocytes, which can result in evasion of immune responses and facilitation of virus replication by inhibition of JAK–STAT signaling (32, 37). These findings indicate that it may be harmful to administer SOCS1 DNA in the acute phase of infectious myocarditis because it may augment viral replication by inhibition of IFN signaling. The effect of SOCS1 transduction on viral myocarditis has been examined by Yasukawa et al. (32). The SOCS1-transgenic mice infected with CVB3 showed increased myocardial injury, virus replication, and mortality. In contrast, they also showed that SOCS1 inhibition in the heart through adeno-associated virus-mediated expression of dnSOCS1 increased resistance to the acute cardiac injury caused by CVB3 infection. These results were acceptable because SOCS proteins have emerged as frequent targets of viral exploitation. Furthermore, when administrating JAK inhibitors, such as SOCS, active serious infections should have been resolved before the start of treatment. It is considered to be inappropriate to use JAK inhibitors for a person with infectious disease or their possibility with consideration for complication of infection (38–40). In contrast, the overactive autoimmune responses triggered by microbial pathogens can persist after elimination of infectious pathogens (7). Therefore, we examined the efficacy of SOCS1 transfection by using EAM induced by cardiac autoantigen immunization in the absence of viral infection. In the current study, we clearly showed the efficacy of *Socs1* gene transfer as an immunosuppressive therapy for myocarditis under infectious pathogen-free conditions in an EAM mice model. The results of a recent randomized, double-blind, placebo-controlled study showed that immunosuppressive therapy, including prednisone and azathioprine, was effective in patients with myocarditis and inflammatory cardiomyopathy and without evidence of the myocardial viral genome (41). These findings indicate that *Socs1* gene transfer can be effective to treat some clinical

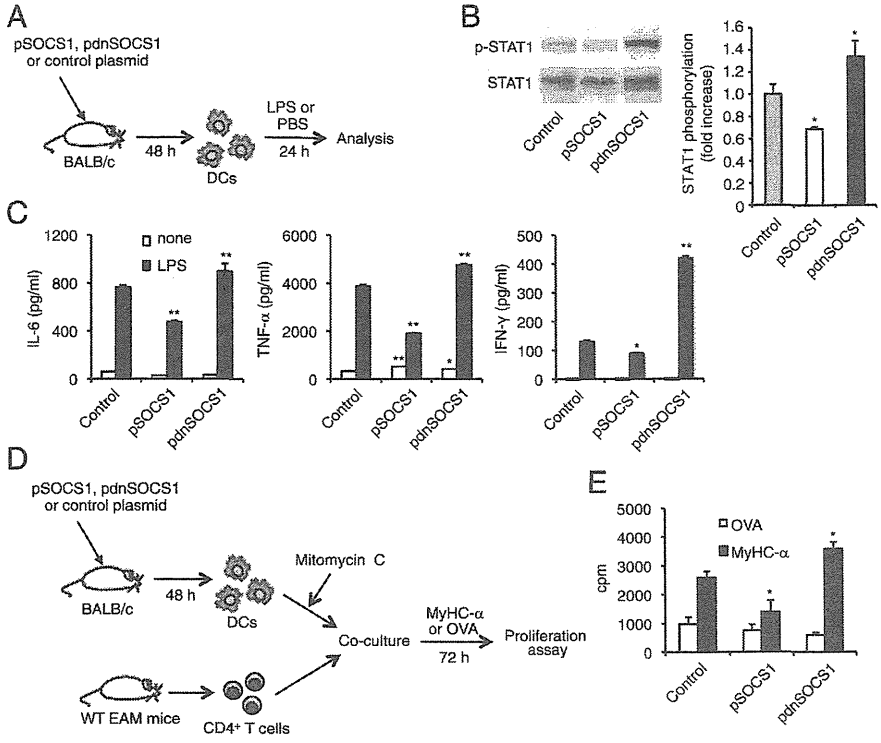

FIGURE 7. Functional capacities of DCs from pSOCS1-, pdnSOCS1-, and control plasmid-treated mice. (**A**) DCs from mice treated with pSOCS1, pdnSOCS1, or control plasmid were stimulated with LPS for 24 h. (**B**) STAT1 phosphorylation of DCs was assessed by Western blotting. Densitometry ratios of pSTAT1/STAT1 are shown as fold induction, the ratio for DCs from control plasmid-injected mice being set at 1. Results are means of five independent experiments ± SEM. Blots are representative of experiments performed a minimum of three times. (**C**) IL-6, TNF-α, and IFN-γ in the culture supernatants were measured by ELISA. Values indicate means ± SEM of triplicate culture wells from one of three independent experiments. (**D** and **E**) Heart-specific $CD4^+$ T cells from EAM mice were restimulated with MyHC-α or OVA peptide on DCs from mice treated with control plasmid, pSOCS1, or pdnSOCS1 for 72 h before measurement of [^{3}H]thymidine incorporation. Each value represents mean ± SEM cpm values of six different culture wells. Results of one of three representative experiments are shown. $*p < 0.05$, $**p < 0.01$ compared with control.

cases of myocarditis and inflammatory cardiomyopathy associated with autoimmunity and without the virus genome in the myocardium, as well as EAM in mice.

In the current study, we demonstrated that the administration of plasmid DNA encoding SOCS1 did not affect autoreactive $CD4^+$ T cell function (Fig. 6) and adoptive transfer of autoreactive $CD4^+$ T cells was able to induce myocarditis in SOCS1 DNA-administered SCID mice (Fig. 8A–D), suggesting that SOCS1 DNA does not suppress either $CD4^+$ T cell recruitment or accumulation of other inflammatory cells in the heart. In contrast, the introduced SOCS1 DNA inhibited the activation of DCs producing proinflammatory cytokines (Fig. 7C). In fact, inhibition of the phosphorylation of STAT1 molecules was observed in DCs from mice injected with SOCS1 DNA (Fig. 7B). In addition, the proliferative responses of $CD4^+$ T cells cocultured with DCs from pSOCS1-treated mice were much weaker than those of cells cultured with DCs from control plasmid-injected mice (Fig. 7E). These results suggest that the inoculated SOCS1 DNA may have been transfected into DCs and impaired DC function in vivo. Contrary to expectations, we could not find evidence of direct transfection of inoculated DNA into DCs in the heart, spleen, peritoneal cavity, or lymph nodes. Although the introduced DNA is expressed predominantly by somatic cells (e.g., cardiomyocytes, keratinocytes, and fibroblasts), it is known that relatively small but biologically significant numbers of DCs are transfected with the inoculated DNA (42–44). Based on this fact, the inoculated SOCS1 DNA may have inhibited DC activation through the direct transfection into DCs; however, our data do not exclude the possibility of another indirect mechanisms.

In the EAM model, activation of TLRs on self-Ag–presenting DCs is essential for the expansion of autoreactive $CD4^+$ T cells to induce myocarditis and heart failure (15). We previously reported that *Tlr4* mutant C3H/HeJ mice are resistant to development of EAM (45). Furthermore, IL-1 type 1 receptor signaling on DCs is critical for autoimmune myocarditis development (11). MyD88 is a crucial common adaptor molecule that mediates both TLRs and IL-1 type 1 receptor activation (46, 47), and MyD88 signaling in DCs is critical for the induction of EAM (16). SOCS1 negatively regulates the MyD88-dependent pathway by interacting with both IL-1R–associated kinase and NF-κB (17), which results in a decrease in the induction of inflammatory cytokines such as TNF-α and IL-6. In fact, production of these inflammatory cytokines was inhibited by the administration of SOCS1 DNA in the current study (Fig. 7C). Although nearly all TLRs recruit MyD88, other specific adaptor proteins function downstream of particular TLRs. One such adaptor molecule is Toll/IL-1R domain-containing adaptor protein/Mal. SOCS1 also binds to tyrosine-phosphorylated Mal through its interaction with Bruton's tyrosine kinase, leading to the suppression of Mal-dependent p65 phosphorylation and transactivation of NF-κB (48). Another important mechanism of the suppression of APC activation by SOCS1 is inhibition of the secondary activated JAK–STAT pathway (49, 50). The Toll/IL-1R domain-containing adaptor protein-inducing IFN-β–IFN-regulatory factor 3 pathway rapidly induces IFN-β, which in turn activates JAK–STAT1 and contributes to the expression of IFN-

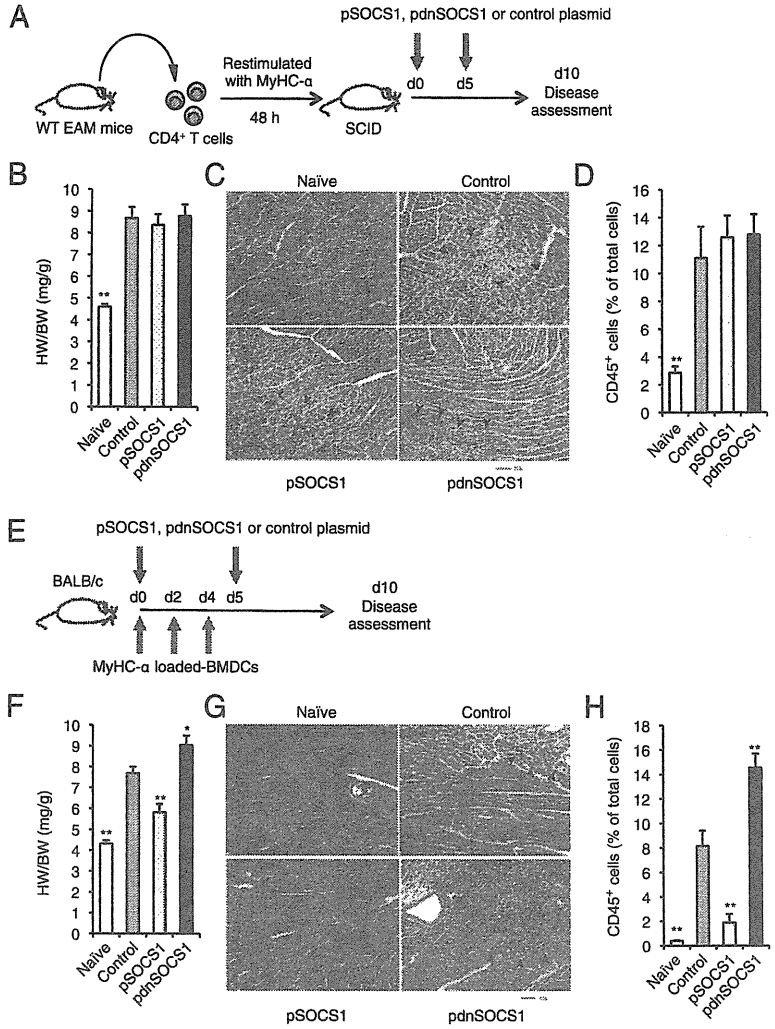

FIGURE 8. pSOCS1 administration inhibited the development of myocarditis induced by cardiac Ag-loaded BMDC injection but not by heart-specific $CD4^+$ T cells. (**A–D**) $CD4^+$ T cells were purified from diseased mice and restimulated in vitro with MyHC-α for 48 h before transfer into SCID recipients. pSOCS1, pdnSOCS1, or control plasmid was injected on days 0 and 5 after the transfer. Heart-to-body weight ratios (B; $n = 5$ mice/group), representative H&E-stained sections of hearts (C), and results of flow cytometry analysis of $CD45^+$ heart infiltrates (D; $n = 5$ mice/group) of naive and adoptive transferred mice at day 10. Arrowheads indicate infiltrating cells. Scale bar, 50 μm. (**E–H**) Mice were immunized with activated MyHC-α– or control OVA peptide-pulsed DCs on days 0, 2, and 4. Mice immunized with MyHC-α–pulsed DCs were treated with pSOCS1, pdnSOCS1, or control plasmid on days 0 and 5. Heart-to-body weight ratios (F; $n = 6$–12 mice/group), representative H&E-stained sections of hearts (G), and results of flow cytometry analysis of $CD45^+$ heart infiltrates (H; $n = 5$ mice/group) of naive and transferred mice at day 10. Arrowheads indicate infiltrating cells. Scale bar, 50 μm. Data are expressed as means ± SEM. Data are representative of at least two independent experiments. $^*p < 0.05$, $^{**}p < 0.01$ compared with control.

inducible genes (51). Moreover, Kimura et al. (52) showed that LPS can activate JAK2 and STAT5, which are involved in IL-6 induction, and that SOCS1 selectively inhibits this process. Thus, SOCS1 negatively regulates several activation pathways in DCs. The present study indicates that pSOCS1 administration is a possible therapy against various diseases caused by overshooting of DCs.

IFN-γ has been shown to be a downregulatory cytokine, as evidenced by exacerbated myocarditis in IFN-γR knockout (KO), IFN-γ KO, and T-bet KO mice (9, 53, 54). In contrast, Th17 cells have recently been implicated in the pathogenesis of various types of autoimmune diseases (reviewed in Ref. 55); however, IL-17 deficiency did not significantly impact the severity of EAM (56). Though these gene-ablated mice provided us with much important information, these studies do not necessarily lead to an effective therapy. In this study, we showed that SOCS1 DNA administration inhibited a broad array of cytokine production from $CD4^+$ T cells (Fig. 4B) and effectively reduced myocardial inflammation (Fig. 1). Compared with inhibition of a single cytokine, SOCS1 DNA therapy could be a more useful therapy that inhibits various signaling pathways to induce production of cytokines.

In the current study, SOCS1 DNA administration was efficacious against EAM development, and inhibition of SOCS1 molecules by SOCS1 antagonist DNA administration enhanced the severity of myocarditis. We demonstrated that SOCS1 DNA administration inhibits the stimulation of self-Ag–presenting DCs inducing cardiac myosin-specific $CD4^+$ T cell responses in peripheral compartments in vivo. Given the availability of clinically effective drugs targeting SOCS1, our findings show new therapeutic perspectives for the treatment of autoimmune myocarditis and cardiomyopathy.

Acknowledgments

We thank T. Okamura, Y. Shiogama, T. Wada, K. Watanabe, H. Shibata, and M. Namikata for technical support and valuable discussion and F. Miyamasu of the Medical English Communications Center, University of Tsukuba, for grammatical revision of this manuscript.

Disclosures

The authors have no financial conflicts of interest.

References

1. Brown, C. A., and J. B. O'Connell. 1995. Myocarditis and idiopathic dilated cardiomyopathy. *Am. J. Med.* 99: 309–314.
2. Feldman, A. M., and D. McNamara. 2000. Myocarditis. *N. Engl. J. Med.* 343: 1388–1398.
3. Caforio, A. L., N. J. Mahon, F. Tona, and W. J. McKenna. 2002. Circulating cardiac autoantibodies in dilated cardiomyopathy and myocarditis: pathogenetic and clinical significance. *Eur. J. Heart Fail.* 4: 411–417.
4. Lauer, B., M. Schannwell, U. Kühl, B. E. Strauer, and H. P. Schultheiss. 2000. Antimyosin autoantibodies are associated with deterioration of systolic and diastolic left ventricular function in patients with chronic myocarditis. *J. Am. Coll. Cardiol.* 35: 11–18.
5. Frustaci, A., C. Chimenti, F. Calabrese, M. Pieroni, G. Thiene, and A. Maseri. 2003. Immunosuppressive therapy for active lymphocytic myocarditis: virological and immunologic profile of responders versus nonresponders. *Circulation* 107: 857–863.
6. Caforio, A. L., J. H. Goldman, A. J. Haven, K. M. Baig, L. D. Libera, and W. J. McKenna; The Myocarditis Treatment Trial Investigators. 1997. Circulating cardiac-specific autoantibodies as markers of autoimmunity in clinical and biopsy-proven myocarditis. *Eur. Heart J.* 18: 270–275.
7. Fairweather, D., Z. Kaya, G. R. Shellam, C. M. Lawson, and N. R. Rose. 2001. From infection to autoimmunity. *J. Autoimmun.* 16: 175–186.
8. Eriksson, U., M. O. Kurrer, W. Sebald, F. Brombacher, and M. Kopf. 2001. Dual role of the IL-12/IFN-gamma axis in the development of autoimmune myocarditis: induction by IL-12 and protection by IFN-gamma. *J. Immunol.* 167: 5464–5469.
9. Afanasyeva, M., Y. Wang, Z. Kaya, E. A. Stafford, K. M. Dohmen, A. A. Sadighi Akha, and N. R. Rose. 2001. Interleukin-12 receptor/STAT4 signaling is required for the development of autoimmune myocarditis in mice by an interferon-gamma-independent pathway. *Circulation* 104: 3145–3151.
10. Eriksson, U., M. O. Kurrer, N. Schmitz, S. C. Marsch, A. Fontana, H. P. Eugster, and M. Kopf. 2003. Interleukin-6-deficient mice resist development of autoimmune myocarditis associated with impaired upregulation of complement C3. *Circulation* 107: 320–325.
11. Eriksson, U., M. O. Kurrer, I. Sonderegger, G. Iezzi, A. Tafuri, L. Hunziker, S. Suzuki, K. Bachmaier, R. M. Bingisser, J. M. Penninger, and M. Kopf. 2003. Activation of dendritic cells through the interleukin 1 receptor 1 is critical for the induction of autoimmune myocarditis. *J. Exp. Med.* 197: 323–331.
12. Sonderegger, I., G. Iezzi, R. Maier, N. Schmitz, M. Kurrer, and M. Kopf. 2008. GM-CSF mediates autoimmunity by enhancing IL-6-dependent Th17 cell development and survival. *J. Exp. Med.* 205: 2281–2294.
13. Satoh, M., G. Tamura, I. Segawa, A. Tashiro, K. Hiramori, and R. Satodate. 1996. Expression of cytokine genes and presence of enteroviral genomic RNA in endomyocardial biopsy tissues of myocarditis and dilated cardiomyopathy. *Virchows Arch.* 427: 503–509.
14. Eriksson, U., and J. M. Penninger. 2005. Autoimmune heart failure: new understandings of pathogenesis. *Int. J. Biochem. Cell Biol.* 37: 27–32.
15. Eriksson, U., R. Ricci, L. Hunziker, M. O. Kurrer, G. Y. Oudit, T. H. Watts, I. Sonderegger, K. Bachmaier, M. Kopf, and J. M. Penninger. 2003. Dendritic cell-induced autoimmune heart failure requires cooperation between adaptive and innate immunity. *Nat. Med.* 9: 1484–1490.
16. Marty, R. R., S. Dirnhofer, N. Mauermann, S. Schweikert, S. Akira, L. Hunziker, J. M. Penninger, and U. Eriksson. 2006. MyD88 signaling controls autoimmune myocarditis induction. *Circulation* 113: 258–265.
17. Dimitriou, I. D., L. Clemenza, A. J. Scotter, G. Chen, F. M. Guerra, and R. Rottapel. 2008. Putting out the fire: coordinated suppression of the innate and adaptive immune systems by SOCS1 and SOCS3 proteins. *Immunol. Rev.* 224: 265–283.
18. Yoshimura, A., T. Naka, and M. Kubo. 2007. SOCS proteins, cytokine signalling and immune regulation. *Nat. Rev. Immunol.* 7: 454–465.
19. Shuai, K., and B. Liu. 2003. Regulation of JAK-STAT signalling in the immune system. *Nat. Rev. Immunol.* 3: 900–911.
20. Croker, B. A., H. Kiu, and S. E. Nicholson. 2008. SOCS regulation of the JAK/STAT signalling pathway. *Semin. Cell Dev. Biol.* 19: 414–422.
21. Fujimoto, M., and T. Naka. 2010. SOCS1, a Negative Regulator of Cytokine Signals and TLR Responses, in Human Liver Diseases. *Gastroenterol. Res. Pract.* 2010: 2010.
22. Naka, T., M. Fujimoto, H. Tsutsui, and A. Yoshimura. 2005. Negative regulation of cytokine and TLR signalings by SOCS and others. *Adv. Immunol.* 87: 61–122.
23. Hanada, T., H. Yoshida, S. Kato, K. Tanaka, K. Masutani, J. Tsukada, Y. Nomura, H. Mimata, M. Kubo, and A. Yoshimura. 2003. Suppressor of cytokine signaling-1 is essential for suppressing dendritic cell activation and systemic autoimmunity. *Immunity* 19: 437–450.
24. Kinjyo, I., T. Hanada, K. Inagaki-Ohara, H. Mori, D. Aki, M. Ohishi, H. Yoshida, M. Kubo, and A. Yoshimura. 2002. SOCS1/JAB is a negative regulator of LPS-induced macrophage activation. *Immunity* 17: 583–591.
25. Nakagawa, R., T. Naka, H. Tsutsui, M. Fujimoto, A. Kimura, T. Abe, E. Seki, S. Sato, O. Takeuchi, K. Takeda, et al. 2002. SOCS-1 participates in negative regulation of LPS responses. *Immunity* 17: 677–687.
26. Lutz, M. B., N. Kukutsch, A. L. Ogilvie, S. Rössner, F. Koch, N. Romani, and G. Schuler. 1999. An advanced culture method for generating large quantities of highly pure dendritic cells from mouse bone marrow. *J. Immunol. Methods* 223: 77–92.
27. Valaperti, A., R. R. Marty, G. Kania, D. Germano, N. Mauermann, S. Dirnhofer, B. Leimenstoll, P. Blyszczuk, C. Dong, C. Mueller, et al. 2008. CD11b+ monocytes abrogate Th17 CD4+ T cell-mediated experimental autoimmune myocarditis. *J. Immunol.* 180: 2686–2695.
28. Cihakova, D., J. G. Barin, M. Afanasyeva, M. Kimura, D. Fairweather, M. Berg, M. V. Talor, G. C. Baldeviano, S. Frisancho, K. Gabrielson, et al. 2008. Interleukin-13 protects against experimental autoimmune myocarditis by regulating macrophage differentiation. *Am. J. Pathol.* 172: 1195–1208.
29. Hanada, T., T. Yoshida, I. Kinjyo, S. Minoguchi, H. Yasukawa, S. Kato, H. Mimata, Y. Nomura, Y. Seki, M. Kubo, and A. Yoshimura. 2001. A mutant form of JAB/SOCS1 augments the cytokine-induced JAK/STAT pathway by accelerating degradation of wild-type JAB/CIS family proteins through the SOCS-box. *J. Biol. Chem.* 276: 40746–40754.
30. Chong, M. M., D. Metcalf, E. Jamieson, W. S. Alexander, and T. W. Kay. 2005. Suppressor of cytokine signaling-1 in T cells and macrophages is critical for preventing lethal inflammation. *Blood* 106: 1668–1675.
31. Ortiz-Muñoz, G., J. L. Martin-Ventura, P. Hernandez-Vargas, B. Mallavia, V. Lopez-Parra, O. Lopez-Franco, B. Muñoz-Garcia, P. Fernandez-Vizarra, L. Ortega, J. Egido, and C. Gomez-Guerrero. 2009. Suppressors of cytokine signaling modulate JAK/STAT-mediated cell responses during atherosclerosis. *Arterioscler. Thromb. Vasc. Biol.* 29: 525–531.
32. Yasukawa, H., T. Yajima, H. Duplain, M. Iwatate, M. Kido, M. Hoshijima, M. D. Weitzman, T. Nakamura, S. Woodard, D. Xiong, et al. 2003. The suppressor of cytokine signaling-1 (SOCS1) is a novel therapeutic target for enterovirus-induced cardiac injury. *J. Clin. Invest.* 111: 469–478.
33. Kanzaki, Y., F. Terasaki, M. Okabe, T. Hayashi, H. Toko, H. Shimomura, S. Fujioka, Y. Kitaura, K. Kawamura, Y. Horii, et al. 2001. Myocardial inflammatory cell infiltrates in cases of dilated cardiomyopathy as a determinant of outcome following partial left ventriculectomy. *Jpn. Circ. J.* 65: 797–802.
34. Münz, C., J. D. Lünemann, M. T. Getts, and S. D. Miller. 2009. Antiviral immune responses: triggers of or triggered by autoimmunity? *Nat. Rev. Immunol.* 9: 246–258.
35. Baetz, A., S. Zimmermann, and A. H. Dalpke. 2007. Microbial immune evasion employing suppressor of cytokine signaling (SOCS) proteins. *Inflamm. Allergy Drug Targets* 6: 160–167.
36. Akhtar, L. N., and E. N. Benveniste. 2011. Viral exploitation of host SOCS protein functions. *J. Virol.* 85: 1912–1921.
37. Yajima, T., H. Yasukawa, E. S. Jeon, D. Xiong, A. Dorner, M. Iwatate, M. Nara, H. Zhou, D. Summers-Torres, M. Hoshijima, et al. 2006. Innate defense mechanism against virus infection within the cardiac myocyte requiring gp130-STAT3 signaling. *Circulation* 114: 2364–2373.
38. Pesu, M., A. Laurence, N. Kishore, S. H. Zwillich, G. Chan, and J. J. O'Shea. 2008. Therapeutic targeting of Janus kinases. *Immunol. Rev.* 223: 132–142.
39. Yamaoka, K., B. Min, Y. J. Zhou, W. E. Paul, and J. J. O'shea. 2005. Jak3 negatively regulates dendritic-cell cytokine production and survival. *Blood* 106: 3227–3233.
40. Changelian, P. S., D. Moshinsky, C. F. Kuhn, M. E. Flanagan, M. J. Munchhof, T. M. Harris, D. A. Whipple, J. L. Doty, J. Sun, C. R. Kent, et al. 2008. The specificity of JAK3 kinase inhibitors. *Blood* 111: 2155–2157.
41. Frustaci, A., M. A. Russo, and C. Chimenti. 2009. Randomized study on the efficacy of immunosuppressive therapy in patients with virus-negative inflammatory cardiomyopathy: the TIMIC study. *Eur. Heart J.* 30: 1995–2002.
42. Tüting, T., W. J. Storkus, and L. D. Falo, Jr. 1998. DNA immunization targeting the skin: molecular control of adaptive immunity. *J. Invest. Dermatol.* 111: 183–188.
43. Condon, C., S. C. Watkins, C. M. Celluzzi, K. Thompson, and L. D. Falo, Jr. 1996. DNA-based immunization by in vivo transfection of dendritic cells. *Nat. Med.* 2: 1122–1128.
44. Porgador, A., K. R. Irvine, A. Iwasaki, B. H. Barber, N. P. Restifo, and R. N. Germain. 1998. Predominant role for directly transfected dendritic cells in antigen presentation to CD8+ T cells after gene gun immunization. *J. Exp. Med.* 188: 1075–1082.
45. Nishikubo, K., K. Imanaka-Yoshida, S. Tamaki, M. Hiroe, T. Yoshida, Y. Adachi, and Y. Yasutomi. 2007. Th1-type immune responses by Toll-like receptor 4 signaling are required for the development of myocarditis in mice with BCG-induced myocarditis. *J. Autoimmun.* 29: 146–153.
46. Akira, S., and H. Hemmi. 2003. Recognition of pathogen-associated molecular patterns by TLR family. *Immunol. Lett.* 85: 85–95.
47. Li, X., and J. Qin. 2005. Modulation of Toll-interleukin 1 receptor mediated signaling. *J. Mol. Med.* 83: 258–266.
48. Mansell, A., R. Smith, S. L. Doyle, P. Gray, J. E. Fenner, P. J. Crack, S. E. Nicholson, D. J. Hilton, L. A. O'Neill, and P. J. Hertzog. 2006. Suppressor of cytokine signaling 1 negatively regulates Toll-like receptor signaling by mediating Mal degradation. *Nat. Immunol.* 7: 148–155.
49. Gingras, S., E. Parganas, A. de Pauw, J. N. Ihle, and P. J. Murray. 2004. Re-examination of the role of suppressor of cytokine signaling 1 (SOCS1) in the regulation of toll-like receptor signaling. *J. Biol. Chem.* 279: 54702–54707.
50. Baetz, A., M. Frey, K. Heeg, and A. H. Dalpke. 2004. Suppressor of cytokine signaling (SOCS) proteins indirectly regulate toll-like receptor signaling in innate immune cells. *J. Biol. Chem.* 279: 54708–54715.

51. Qin, H., C. A. Wilson, S. J. Lee, and E. N. Benveniste. 2006. IFN-beta-induced SOCS-1 negatively regulates CD40 gene expression in macrophages and microglia. *FASEB J.* 20: 985–987.
52. Kimura, A., T. Naka, T. Muta, O. Takeuchi, S. Akira, I. Kawase, and T. Kishimoto. 2005. Suppressor of cytokine signaling-1 selectively inhibits LPS-induced IL-6 production by regulating JAK-STAT. *Proc. Natl. Acad. Sci. USA* 102: 17089–17094.
53. Eriksson, U., M. O. Kurrer, R. Bingisser, H. P. Eugster, P. Saremaslani, F. Follath, S. Marsch, and U. Widmer. 2001. Lethal autoimmune myocarditis in interferon-gamma receptor-deficient mice: enhanced disease severity by impaired inducible nitric oxide synthase induction. *Circulation* 103: 18–21.
54. Rangachari, M., N. Mauermann, R. R. Marty, S. Dirnhofer, M. O. Kurrer, V. Komnenovic, J. M. Penninger, and U. Eriksson. 2006. T-bet negatively regulates autoimmune myocarditis by suppressing local production of interleukin 17. *J. Exp. Med.* 203: 2009–2019.
55. Ghoreschi, K., A. Laurence, X. P. Yang, K. Hirahara, and J. J. O'Shea. 2011. T helper 17 cell heterogeneity and pathogenicity in autoimmune disease. *Trends Immunol.* 32: 395–401.
56. Baldeviano, G. C., J. G. Barin, M. V. Talor, S. Srinivasan, D. Bedja, D. Zheng, K. Gabrielson, Y. Iwakura, N. R. Rose, and D. Cihakova. 2010. Interleukin-17A is dispensable for myocarditis but essential for the progression to dilated cardiomyopathy. *Circ. Res.* 106: 1646–1655.

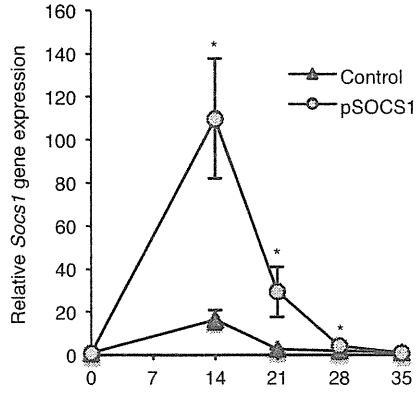

Supplementary Figure 1. *Socs1* gene expression in the heart. RNA samples were obtained from EAM hearts on days 0, 14, 21, 28 and 35, and used as a template for QRT-PCR. Results represent the average gene induction in five to six independent heart samples. Results of one of two representative experiments are shown. $*P < 0.05$ compared to control.

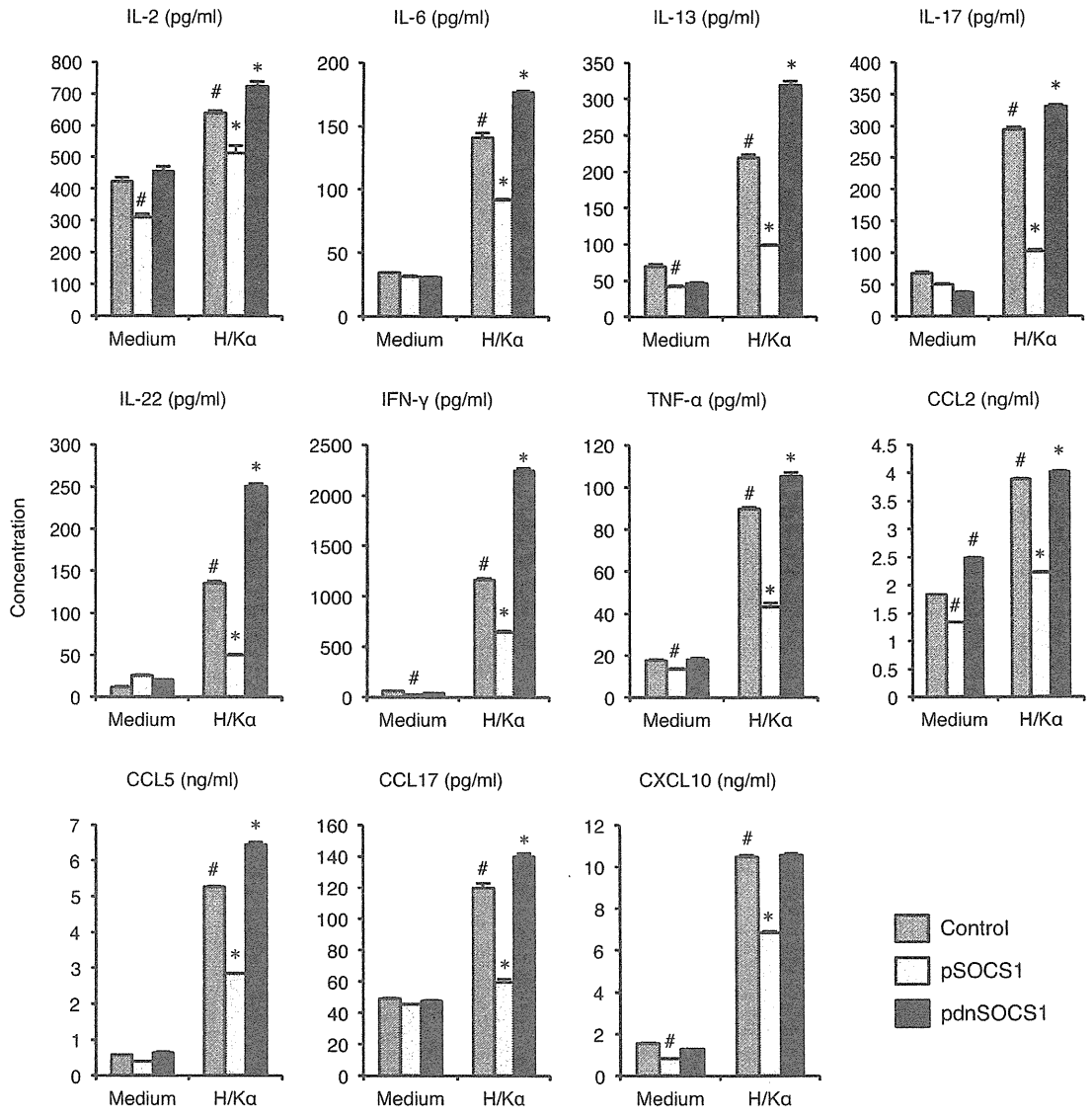

Supplementary Figure 2. Impaired cytokine production by H^+/K^+ ATPase α (H/Kα)-specific $CD4^+$ T cells in pSOCS1-treated mice. BALB/c mice were immunized twice, on days 0 and 7, with 100 μg of H/Kα p253-277 in an emulsion with CFA and treated with pSOCS1, pdnSOCS1 or control plasmid on days 0, 5 and 10. Splenocytes were isolated from mice on day 14 and cultured in the absence or presence of H/Kα peptide (1 μg/ml) for 72 h. Cytokines and chemokines in the culture supernatants were measured by ELISA. Data are expressed as mean ± SEM from triplicate culture wells. Results of one of two representative experiments are shown. *$P < 0.05$ compared to H/Kα stimulated control and #$P < 0.05$ compared to unstimulated control.

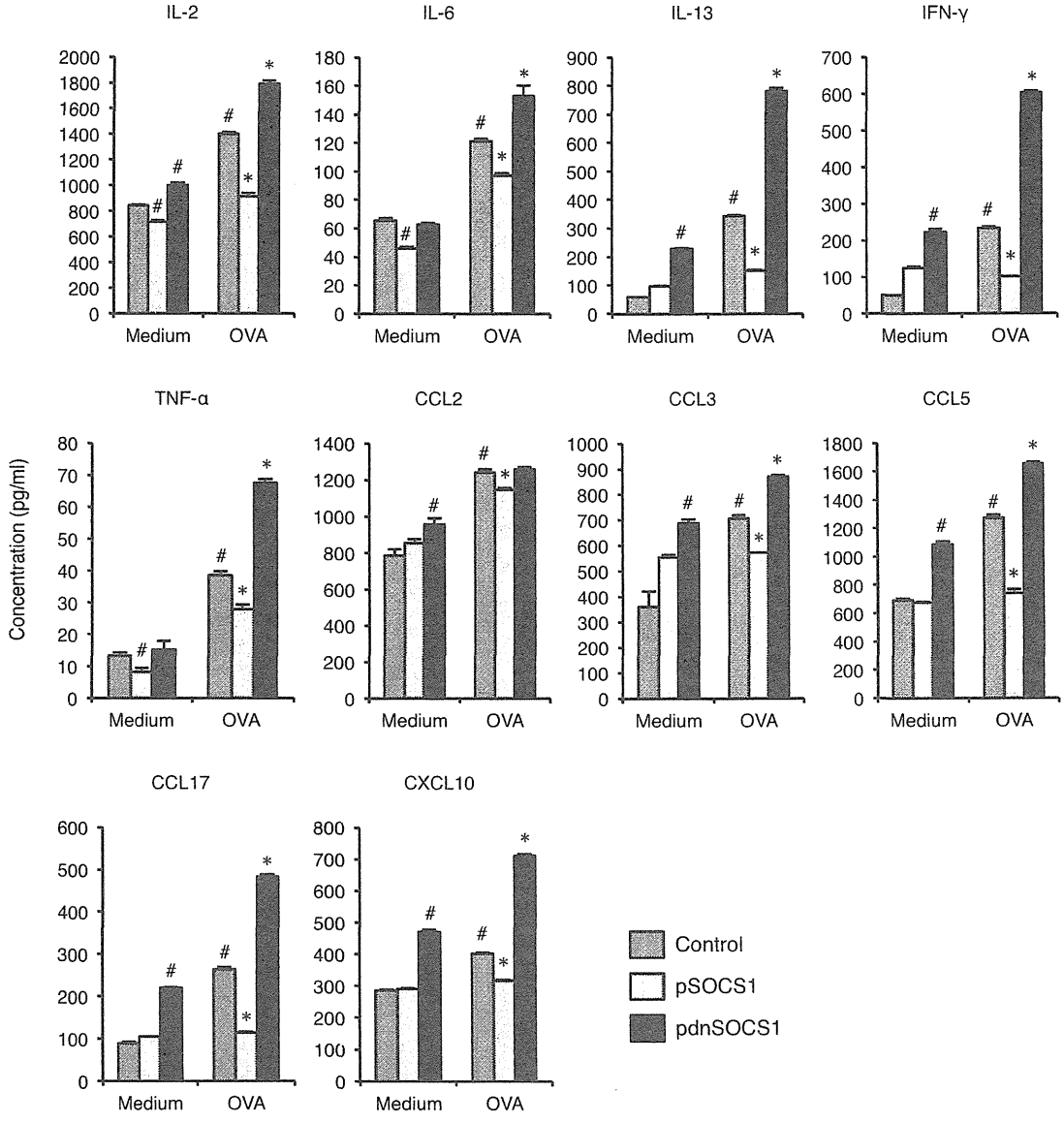

Supplementary Figure 3. Impaired cytokine production by OVA-specific CD4$^+$ T cells in pSOCS1-treated mice. BALB/c mice were immunized twice, on days 0 and 7, with 100 μg of OVA p323-339 in an emulsion with alum and treated with pSOCS1, pdnSOCS1 or control plasmid on days 0, 5 and 10. Splenocytes were isolated from mice on day 14 and cultured in the absence or presence of OVA peptide (5 μg/ml) for 72 h. Cytokines and chemokines in the culture supernatants were measured by ELISA. Data are expressed as mean ± SEM from triplicate culture wells. Results of one of two representative experiments are shown. *$P < 0.05$ compared to OVA stimulated control and #$P < 0.05$ compared to unstimulated control.

doi:10.1093/brain/awr348 Brain 2012: 135; 833–846 | 833

BRAIN
A JOURNAL OF NEUROLOGY

Non-human primate model of amyotrophic lateral sclerosis with cytoplasmic mislocalization of TDP-43

Azusa Uchida,[1] Hiroki Sasaguri,[1] Nobuyuki Kimura,[2] Mio Tajiri,[1] Takuya Ohkubo,[1] Fumiko Ono,[3] Fumika Sakaue,[1] Kazuaki Kanai,[4] Takashi Hirai,[5] Tatsuhiko Sano,[1] Kazumoto Shibuya,[4] Masaki Kobayashi,[1] Mariko Yamamoto,[1] Shigefumi Yokota,[1] Takayuki Kubodera,[1] Masaki Tomori,[5] Kyohei Sakaki,[5] Mitsuhiro Enomoto,[5] Yukihiko Hirai,[6] Jiro Kumagai,[7] Yasuhiro Yasutomi,[2] Hideki Mochizuki,[8] Satoshi Kuwabara,[4] Toshiki Uchihara,[9] Hidehiro Mizusawa[1] and Takanori Yokota[1]

1 Department of Neurology and Neurological Science, Graduate School of Medicine, Tokyo Medical and Dental University, Tokyo 113-8519, Japan
2 Tsukuba Primate Research Centre, National Institute of Biomedical Innovation, Tsukuba 305-0843, Japan
3 Corporation for Production and Research of Laboratory Primates, Tsukuba 305-0843, Japan
4 Department of Neurology, Graduate School of Medicine, Chiba University, Chiba 260-8670, Japan
5 Department of Orthopaedic Surgery, Graduate School of Medicine, Tokyo Medical and Dental University, Tokyo 113-8519, Japan
6 Department of Biochemistry and Molecular Biology, Nippon Medical School, Tokyo 113-8602, Japan
7 Department of Pathology, Graduate School of Medicine, Tokyo Medical and Dental University, Tokyo 113-8519, Japan
8 Department of Neurology, Kitasato University School of Medicine, Kanagawa 228-8555, Japan
9 Laboratory of Structural Neuropathology, Tokyo Metropolitan Institute of Medical Science, Tokyo 156-8506, Japan

Correspondence to: Takanori Yokota,
Department of Neurology and Neurological Science,
Graduate School of Medicine,
Tokyo Medical and Dental University,
Bunkyo-ku, Tokyo 113-8519,
Japan
E-mail: tak-yokota.nuro@tmd.ac.jp

Amyotrophic lateral sclerosis is a fatal neurodegenerative disease characterized by progressive motoneuron loss. Redistribution of transactive response deoxyribonucleic acid-binding protein 43 from the nucleus to the cytoplasm and the presence of cystatin C-positive Bunina bodies are considered pathological hallmarks of amyotrophic lateral sclerosis, but their significance has not been fully elucidated. Since all reported rodent transgenic models using wild-type transactive response deoxyribonucleic acid-binding protein 43 failed to recapitulate these features, we expected a species difference and aimed to make a non-human primate model of amyotrophic lateral sclerosis. We overexpressed wild-type human transactive response deoxyribonucleic acid-binding protein 43 in spinal cords of cynomolgus monkeys and rats by injecting adeno-associated virus vector into the cervical cord, and examined the phenotype using behavioural, electrophysiological, neuropathological and biochemical analyses. These monkeys developed progressive motor weakness and muscle atrophy with fasciculation in distal hand muscles first. They also showed regional cytoplasmic transactive response deoxyribonucleic acid-binding protein 43 mislocalization with loss of nuclear transactive response deoxyribonucleic acid-binding protein 43 staining in the lateral nuclear group of spinal cord innervating distal hand muscles and cystatin C-positive cytoplasmic aggregates, reminiscent of the spinal cord pathology of patients with amyotrophic lateral sclerosis. Transactive response deoxyribonucleic acid-binding protein 43 mislocalization was

Received July 27, 2011. Revised October 26, 2011. Accepted November 14, 2011. Advance Access publication January 17, 2012

an early or presymptomatic event and was later associated with neuron loss. These findings suggest that the transactive response deoxyribonucleic acid-binding protein 43 mislocalization leads to α-motoneuron degeneration. Furthermore, truncation of transactive response deoxyribonucleic acid-binding protein 43 was not a prerequisite for motoneuronal degeneration, and phosphorylation of transactive response deoxyribonucleic acid-binding protein 43 occurred after degeneration had begun. In contrast, similarly prepared rat models expressed transactive response deoxyribonucleic acid-binding protein 43 only in the nucleus of motoneurons. There is thus a species difference in transactive response deoxyribonucleic acid-binding protein 43 pathology, and our monkey model recapitulates amyotrophic lateral sclerosis pathology to a greater extent than rodent models, providing a valuable tool for studying the pathogenesis of sporadic amyotrophic lateral sclerosis.

Keywords: TDP-43; Bunina bodies; cystatin C; cynomolgus monkeys; amyotrophic lateral sclerosis

Abbreviations: AAV = adeno-associated virus; ALS = amyotrophic lateral sclerosis; FTLD = frontotemporal lobar degeneration; HEK = human embryonic kidney; TDP-43 = transactive response DNA-binding protein 43

Introduction

Amyotrophic lateral sclerosis (ALS), also known as Lou Gehrig's disease, is an incurable progressive neurodegenerative disease characterized by muscle weakness and atrophy resulting from the combined loss of upper and lower motoneurons. Most cases of ALS are sporadic, and only 10% of ALS cases are of a familial form. Protein aggregates are one histopathological characteristic of ALS. A breakthrough in understanding ALS pathogenesis was the discovery of the 43-kDa transactive response DNA-binding protein (TDP-43), which was recently identified as the major component of the protein aggregates and of the insoluble fraction in the brains of patients with sporadic ALS and frontotemporal lobar degeneration (FTLD) (Arai *et al.*, 2006; Neumann *et al.*, 2006). TDP-43 is now expected to play an essential role in the pathogenesis of sporadic ALS, possibly equivalent to that of tau and beta amyloid in Alzheimer's disease or α-synuclein in Parkinson's disease.

Human TDP-43 is a highly conserved and ubiquitously expressed 414 amino acid nuclear protein that binds to both DNA and RNA (Ou *et al.*, 1995; Buratti *et al.*, 2001). In normal settings, TDP-43 is a primarily nuclear protein that functions in transcription regulation, alternative splicing and RNA stabilization (Buratti *et al.*, 2008), as well as in microRNA metabolism (Buratti *et al.*, 2010). Pathological TDP-43 can be abnormally truncated, phosphorylated and ubiquitinated, and most TDP-43 is mislocalized from the nucleus to the cytoplasm or neurites (Arai *et al.*, 2006; Neumann *et al.*, 2006). Of note, almost all neurons with cytoplasmic TDP-43 accumulations show a dramatic depletion of normal nuclear TDP-43. Thus, both gain and loss of functions are potential disease mechanisms, either due to the loss of normal nuclear TDP-43 expression, or cytoplasmic mislocalization (Arai *et al.*, 2006; Neumann *et al.*, 2006; Cairns *et al.*, 2007). Therefore, cytoplasmic TDP-43 mislocalization with loss of its nuclear staining is a key feature found in the majority of patients' brains and spinal cords (Arai *et al.*, 2006; Neumann *et al.*, 2006).

TDP-43 strictly regulates its messenger RNA levels by directly binding to an intron in the 3′-untranslated region of its own transcript and enhancing its splicing (Ayala *et al.*, 2010; Polymenidou *et al.*, 2011), however, the expression level of TDP-43 can be upregulated ~1.5-fold (Mishra *et al.*, 2007; Gitcho *et al.*, 2009) in FTLD/ALS. Moreover, mutations in the *TDP-43* gene are associated with familial ALS (Kabashi *et al.*, 2008; Yokoseki *et al.*, 2008), in which TDP-43 is also frequently mislocalized within motoneurons of the spinal cord. These reports support the hypothesis that mislocalization of this protein plays a central role in the disease pathogenesis. The rodent, *Drosophila*, *Ceanorhabditis elegans* and zebrafish models with overexpressed mutant as well as wild-type TDP-43 show severe motor symptoms and wild-type TDP-43 localizes exclusively or primarily to nuclei (Ash *et al.*, 2010; Hanson *et al.*, 2010; Kabashi *et al.*, 2010; Li *et al.*, 2010; Shan *et al.*, 2010; Voigt *et al.*, 2010; Wils *et al.*, 2010; Xu *et al.*, 2010; Swarup *et al.*, 2011), although mutant TDP-43 is more likely to accumulate in the cytoplasm (Swarup *et al.*, 2011). The results of the rodent models suggested that overexpressed nuclear wild-type TDP-43 is toxic, but provide little insight for the significance of mislocalized wild-type TDP-43. Even in mouse models that overexpress wild-type TDP-43 with mutated nuclear localization signals, total human and mouse nuclear TDP-43 was not reduced (Igaz *et al.*, 2011) when compared with that in littermate wild-type controls. Together, these reported mouse models might have a different TDP-43 pathology from that found in patients with ALS. Expecting that a primate model of ALS might more closely reflect the TDP-43 pathology in human patients with ALS, we overexpressed human wild-type TDP-43 in the spinal motoneurons of a non-human primate, the cynomolgus monkey, using an adeno-associated virus (AAV) 1 vector.

Materials and methods

Human subjects

Neurologists clinically diagnosed ALS with the aid of electrophysiological examinations. The clinical diagnosis of definite ALS was based on El Escorial (Brooks *et al.*, 2000) and electrodiagnostic (De Carvalho *et al.*, 2008) criteria and confirmed by neuropathological examination in accordance with published guidelines (Piao *et al.*, 2003).

The patient study protocol was approved by the institutional clinical study committee at Tokyo Medical and Dental University (No. 799). Consent forms for autopsy were obtained from legal representatives of all patients in accordance with the guidelines of the institutional review boards.

Animals

Ten male adult cynomolgus monkeys (*Macaca fascicularis*; 3–7 years old, 3.28–5.10 kg) were bred and treated at Tsukuba Primate Research Centre. The number of monkeys and concentrations of viral stocks were as follows: one monkey was injected with high-dose Flag-TDP-43 AAV1 [1×10^{13} viral genomes (vg)/ml]; six monkeys were injected with low-dose Flag-TDP-43 AAV1 (3×10^{12} vg/ml); three monkeys were injected with low-dose mock AAV1 (3×10^{12} vg/ml) as a negative control. Three monkeys injected with low-dose TDP-43 AAV1 were pathologically examined in the early stage, 3–5 days after the onset of motor symptoms and the other three monkeys were examined in the late stage, 4–7 weeks after injection.

Eleven adult male Fisher rats (10 weeks old, Sankyo-lab) were used. The number of rats and concentrations of viral stocks were as follows: eight rats were injected with low-dose Flag-TDP-43 AAV1 (3×10^{12} vg/ml) and three rats were injected with low-dose control AAV1 (3×10^{12} vg/ml) as a negative control. Three rats injected with TDP-43 AAV1 were pathologically examined in the early stage, 1–2 weeks after injection, and the others were examined in the late stage, 4–9 weeks after injection.

All animal experiments were conducted according to the U.S. National Institutes of Health Guide for the Care and Use of Laboratory Animals, and the Guidelines for the Animal Care and Management of the Tsukuba Primate Research Center and Tokyo Medical and Dental University.

Constructs

Human wild-type TDP-43 was purchased from Invitrogen. The TDP-43 and Flag-TDP-43 fragments were generated by polymerase chain reaction using the following primer pairs: 5′-CCGCTCGAGGCCACCATG GATTAC AAGGATGACGACGATAAGTCTGAATATATTCGGGTAA CCGG-3′ and 5′-CCGCTCGAGCTACATTCCCCAG CCAGAAG ACTTA-3′ for TDP-43, and 5′-CCGCTCGAGGCCACCATGGATTACA AGGATGACGACGAT AAGTCTGAATATATTCGGGTAACCGG-3′ and 5′-CCGCTCGAGCTACATTCCCCAGCCAGAAGACTTA-3′ for Flag-TDP-43, which contained XhoI digestion sites at the 3′- and 5′-ends. The Flag-TDP-43 complementary DNA was subcloned into an expression cassette flanked with AAV2 inverted terminal repeats (Stratagene). The cytomegalovirus (CMV) promoter was used to drive expression.

Adeno-associated virus preparations

Human embryonic kidney (HEK) 293 cells at ~70% confluence were transfected with the AAV1 packaging plasmid pRep2/Cap9 (gift from Dr James M. Wilson, University of Pennsylvania) and adenovirus helper plasmid (Stratagene) at a ratio of 1:1:1. At 6 h after transfection, the culture medium was replaced with fresh medium, and the cells were incubated for 48 h. The cells were then harvested from the culture dishes and pelleted by centrifugation, resuspended in phosphate-buffered saline and subjected to three rounds of freeze–thawing. Cell debris was then pelleted by centrifugation at 1200*g* for 15 min. AAV vectors were purified using ammonium sulphate precipitation and iodixanol (Axis-Shield) continuous gradient centrifugation.

Size-exclusion chromatography was performed using an AKTA Explorer 100 HPLC system (GE Healthcare) equipped with a 2-ml sample loop. A Superdex 200 10/300 GL column (GE Healthcare) was equilibrated with MHA buffer (3.3 mM MES, 3.3 mM HEPES, 3.3 mM NaOAc, 50 mM NaCl, pH 6.5). The vector-containing fractions were loaded onto the column at a flow rate of 0.5 ml/min, and the eluate was collected as 0.5 ml fractions over the duration of one column volume (23 ml). AAV peak fractions were identified by 280/260 nm absorbance and real-time quantitative polymerase chain reaction using vector-specific primers. The purified AAVs were then concentrated further by using Amico Ultra-4 tubes (Ultracel-30k, Millipore) to a final concentration of 1×10^{13} genome copies/ml, as determined by real-time quantitative polymerase chain reaction.

The genome copy number was calculated by TaqMan® PCR (Applied Biosystems). The vectors were treated with Benzonase® and digested with proteinase K (Wako Pure Chemical Industries) for 1 h and purified by phenol–chloroform extraction. The TaqMan® primers and probe were designed as follows: forward primer: 5′-CAGGCTGGT CCAACTCCTA-3′, reverse primer: 5′-GCAGTGGTTCACGCCTGTAA-3′, and probe: 5′-TACCCACCTTGGCCTC-3′. The designed TaqMan® PCR fragment was located in the human growth hormone polyadenylation site in the vector.

Successful viral assembly of control AAV and transgene expression were confirmed by immunoblot analysis using HEK 293 cells infected with AAV (Supplementary Fig. 1), as described below.

HEK-293 cells were cultured in Dulbecco's modified Eagle's medium containing 10% foetal bovine serum with 1% penicillin/streptomycin. The cells in 12-well plates were infected by Flag-TDP-43 AAV1 (5×10^{10} vg/ml). At 48 h after infection, cells were harvested by gentle scraping in lysis buffer [20 mM Tris–HCl, 150 mM NaCl, 1% NP-40, 0.1% deoxicolate, 1% sodium dodecyl sulphate, 1 mM EDTA, 1 mM EGTA, 10 mM β-glycerophosphate, 5 mM NaF and Complete protease inhibitor cocktail (Roche Diagnostics)]. Equal amounts of total cellular protein were mixed with 5× Laemmli sample buffer, denatured at 95°C for 5 min, and separated with 10% sodium dodecyl sulphate polyacrylamide gel electrophoresis. The proteins were transferred to PVDF membranes. After blocking with 3% gelatin (Wako Pure Chemical Industry) in Tris-buffered saline or 5% skimmed milk (Wako Pure Chemical Industry) in Tris-buffered saline-Triton X-100, the membranes were incubated overnight with the following primary antibodies: anti-M2 (1:2000); anti-pan-TDP-43 (1:2000); and anti-VP1, VP2 and VP3 of AAV (1:1000). After incubation with an appropriate horseradish peroxidase-conjugated secondary antibody (Santa Cruz Biotechnology), labelling was detected with the ECL Plus™ Chemiluminescent Detection System (GE Healthcare) or SuperSignal (Thermo Scientific).

Stereotaxic injection of adeno-associated viral vectors

All surgical operations were performed under general anaesthesia. Ketamine hydrochloride (Ketalar, Sankyo) was intramuscularly administered at a dose of 5 mg/kg as a pre-anaesthetic agent, and general anaesthesia was maintained with isoflurane (Forane, Abbott) and oxygen after tracheal intubation. The monkeys were positioned in a stereotaxic frame. After a bilateral laminectomy and opening the dura in the midline at C5–6, AAV vectors were stereotaxically injected into the side ipsilateral to the dominant hand. The injection site was determined and depth of needle insertion was calculated from the preoperatively taken MRI of cervical spinal cord. AAV stock (5 µl) was injected through a 31-gauge needle connected to a 10-µl Hamilton microsyringe in 2 min. The needle remained in place for 10 min and was removed slowly. The dura and skin were sutured and monkeys returned to their individual cages. The monkeys received 0.5 mg/kg butorphanol tartrate (Stadol, Bristol-Myers Squibb) intramuscularly for 3 days to alleviate any postoperative pain.

The rats were anaesthetized with an intraperitoneally administered cocktail of 1.5 ml chloral hydrate (70 mg/ml, Wako Pure Chemical Industry) and 0.1 ml ketamine hydrochloride (70 mg/ml) at a dose of 6 ml/kg. A left side hemi-laminectomy was performed from C4 to C6. On the left side of the C6 segment, 1.5 µl of viral stock was manually injected through sharpened microcapillary glass (PN-30 puller, Narishige) connected via silicone to a 10-µl Hamilton microsyringe at a rate of 0.5 µl/min. The sharpened microcapillary glass remained in place for 3 min and was removed slowly. The skin was sutured, the rats placed on a heating pad until they began to recover from surgery, and then returned to their individual cages.

For detection of the AAV genome in the spinal cord, total DNA was extracted from spinal cord with homogenized buffer containing 0.5% sodium dodecyl sulphate, 10 mM Tris–HCl pH 8.0, and 10 mM EDTA pH 8.0, and polymerase chain reactions were carried out with the following primer pair: 5′-CGCTGTTTTGACCTCCATAGAA-3′ and 5′-AGGCGGTACTTACGTCACTCTTG-3′ for the cytomegalovirus β-globin intron.

Behavioural analysis

For monkeys, to evaluate weakness of the forelimb muscles on the AAV-injected side (the dominant-hand side), we performed the 'apple test'. The front fence of the cage was altered to have two holes and trays on the right and left side. A piece of apple was placed in line from back (monkey side) to front (observer side) on the left or right tray at 3, 6, 9 and 12 cm from the front fence during a session. The monkeys were trained to reach a small piece of apple on the trays through the hole. Four sessions were performed alternately for each side. We analysed how frequently a monkey used his dominant hand to pick up apples before and every week after the operations. We also carefully observed behaviour of the monkeys in daily life every day and recorded video monitoring for 30 min per week.

For rats, to evaluate weakness of the forelimb muscles, we measured grip strength using a special device (Muromachi Kiki) as previously described (Anderson, 2005).

Electrophysiological assessment

The nerve conduction study and needle EMG studies were performed under anaesthesia with a combination of 7 mg/kg ketamine hydrochloride and 1.2 mg/kg xylazine administrated intramuscularly. Nerve conduction studies were performed in the bilateral median nerves using conventional procedures and an EMG Machine (MEB-2300, Nihon-koden). The recording surface electrode was placed over the belly of the thenar eminence with a reference electrode at the metacarpophalangeal joint of the thumb, and compound muscle action potentials were elicited after the stimulation of the median nerve at the wrist. The peak-to-peak amplitudes were measured for all compound muscle action potentials. Nerve conduction studies were examined before AAV injection and every 1 or 2 weeks after. The needle EMG study was performed in the first dorsal interosseous, flexor carpi ulnaris and biceps brachii muscles using a conventional concentric needle electrode used in human studies (TECA Elite, CareFusion), 4–6 weeks after AAV injection.

Neuropathological examinations

Animals were deeply anaesthetized first with intramuscularly administered 7 mg/kg ketamine hydrochloride and then with intravenously administered 25 mg/kg pentobarbital. After confirming the absence of a blink reflex, the spinal cord and skeletal muscles were removed. For neuropathological examination, human and animal spinal cord samples were immersion fixed in 10% neutral buffered formalin, processed conventionally, embedded in paraffin, cut into 4-µm-thick sections and stained with haematoxylin and eosin. For immunostaining, sections were deparaffinized, pretreated in 0.5% periodic acid, autoclaved for 5 min at 121°C and then incubated free-floating overnight at 4°C with the following primary antibodies: M2 (1:500), anti-pan-TDP-43 (1:1000), anti-pS409/410-TDP-43 (1:500), anti-ubiquitin (1:500), anti-p62 (1:500), anti-cystatin-C (1:1000), anti-GFAP (1:500), anti-GLUT-5 (1:500) and SMI31 (1:200). Following brief washes, the sections were sequentially incubated with polymer immunocomplex (Dako)

Immunoreactive elements were visualized by treating sections with 3,3′ diaminobenzidine tetroxide (DAB-4HCl, Dojin Kagaku) with or without nickel ammonium chloride. The sections were then counterstained with haematoxylin. For double-immunostaining, the deparaffinized sections were stained with Sudan Black B to avoid autofluorescence. The free-floating sections were incubated overnight at 4°C in solutions containing the primary antibodies. The sections were then incubated with AlexaFluor 488- or 555-conjugated secondary antibodies (1:500, Invitrogen), and DAPI nuclear stain (1:500, Santa Cruz Biotechnology) for 1 h. All sections were examined using a confocal microscope (NIKON or Carl Zeiss).

Animal anterior root samples were fixed with a mixture of 2.5% glutaraldehyde in 0.1 M phosphate buffer (pH 7.4) at 4°C overnight, and then further fixed in 1% osmium tetroxide in 0.1 M phosphate buffer (pH 7.4) for 1 h. The well-fixed tissues were dehydrated in graded ethanol and embedded in Epon 812 (Poly/Bed® 812, Polyscience). The fixed roots were transversely cut into 1-µm-thick sections and stained with toluidine blue.

For counting of anterior horn neurons in the spinal cord, monkey eighth cervical segments were serially cut at 4-µm thickness, and every fifth section was stained with haematoxylin and eosin. The previous and next serial sections (that is, every fourth and sixth sections) were immunostained with anti-pan-TDP-43 or anti-Flag antibodies. The number and minimum diameters of neurons with nuclei in the lateral or medial nuclear groups in 15 sections were evaluated using the Image J software program from the U.S. National Institutes of Health.

Antibody information

We used the following primary antibodies for immunostaining and immunoblot analyses: mouse monoclonal anti-Flag (M2, Sigma); rabbit polyclonal anti-pan-TDP-43 (10782-1-AP, ProteinTech Group); rabbit polyclonal anti-C-terminal TDP-43 (12892-1-AP, ProteinTech Group); rabbit polyclonal anti-phosphorylated S409/410 TDP-43 (Cosmo Bio); rabbit polyclonal anti-ubiquitin (Dako); rabbit polyclonal anti-cystatin-C (Dako); mouse monoclonal anti-phosphorylated neurofilament (SMI31, Sternberger Monoclonals); rabbit polyclonal anti-glial fibrillary acidic protein (GFAP) (Dako); rabbit polyclonal anti-glucose transporter 5 (GLUT-5, IBL); rabbit polyclonal and mouse monoclonal anti-peripeherin (AB1530 and AB1527, Chemicon); mouse monoclonal anti-neurofilament light (N5139, Sigma) antibody; anti-p62 (GP62-C, Progen); anti-glyceraldehyde-3-phosphate dehydrogenase (GAPDH, Biodesign), and anti-AAV capsid proteins VP1, VP2 and VP3 (Progen Biotechnik).

Sequential biochemical fractionation, dephosphorylation and immunoblot analysis

Frozen frontal cortex or spinal cord (50–250 mg) was homogenized in 10 volumes of buffer A (10 mM Tris–HCl pH 7.5, containing 1 mM

EGTA, 10% sucrose and 0.8 M NaCl). After the addition of Triton X-100 at a final concentration of 1%, the homogenate was incubated for 30 min at 37°C and spun at 100 000*g* for 20 min at 20°C. The pellet was homogenized in 20 volumes of buffer A containing 1% sarkosyl, incubated for 30 min at 37°C and spun at 100 000*g* for 20 min at 20°C. The sarkosyl-insoluble pellet was homogenized in four volumes of buffer A containing 1% CHAPS [3-[(3-cholamidopropyl)dimethylammonio]-1-propanesulphonate] and spun at 100 000*g* for 20 min. The pellet was sonicated in 0.5 volume of 8 mol/l urea buffer, cleared by centrifugation at 100 000*g* for 20 min at 20°C, and used for immunoblotting. The samples before (−) and after (+) treatment with lambda protein phosphatase (1600 U/ml, New England Biolabs) were subjected to 10% sodium dodecyl sulphate polyacrylamide gel electrophoresis. Proteins in the gel were then transferred onto a polyvinylidene difluoride (PVDF) membrane (Millipore). After blocking with 3% gelatin (Wako Pure Chemical Industries) in Tris-buffered saline (50 mM Tris–HCl pH 7.5, 150 mM NaCl), the membranes were incubated overnight with the following primary antibodies: anti-M2 (1:2000); anti-C-TDP-43 (1:1200); anti-phosphorylated S409/410 TDP-43 (1:2000); anti-p62 (1:3000) and anti-GAPDH (1:2000). After incubation with an appropriate horseradish peroxidase-conjugated secondary antibody (Santa Cruz Biotechnology), labelling was detected by a 3,3′diaminobendizene reaction intensified with nickel chloride (Metal-Enhanced DAB Substrate Kit, Thermo Scientific), the ECL Plus™ Chemiluminescent Detection System (GE Healthcare), or SuperSignal (Thermo Scientific).

Quantitative real-time polymerase chain reaction assay

Total RNA was extracted from whole-brain homogenates with Isogen (Nippon Gene). DNase-treated RNA (2.5 μg) was reverse-transcribed with SuperScript® III and random hexamers (Life Technologies). Complementary DNA was amplified by the quantitative TaqMan® system by using the Light Cycler 480 Real-Time PCR Instrument (Roche Diagnostics). The primers and probes specific for Flag-tagged human TDP-43, rat TDP-43 (NM_001011979.2) and monkey TDP-43 (XM_001102660.2) were designed. Relative Flag-human TDP-43 messenger RNA levels were calculated in comparison to endogenous rat or cynomolgus messenger RNA levels. A list of all primers and probes used in this study is provided in Supplementary Table 1.

Statistical analysis

The data obtained from independent experiments are presented as means ± SEM.

Statistical analysis of spinal neuron counts and axonal density among TDP-43-expressed monkey group in early, late stage and control monkey group by one-way ANOVA with Bonferroni's *post hoc* test. $P < 0.05$ was considered significant.

Results

Overexpressing wild-type TDP-43 in the monkey cervical cord leads to progressive motor weakness and muscle atrophy with fasciculation

AAV expressing Flag-tagged TDP-43 (Supplementary Fig. 2) was directly injected into the sixth cervical segment on the dominant-hand side of seven monkeys. All monkeys developed progressive motor weakness and muscle atrophy with marked fasciculation in the forelimb on the injected side (Fig. 1A and B, Supplementary Video 1). Two to 3 weeks after the injection, the TDP-43-expressing monkeys first showed some difficulty in taking time to pick up pieces of apple using the dominant hand on the injected side in the apple test, and changed to use the non-dominant hand (Fig. 1C). On observation by video monitoring, they could reach and grasp the ceiling fence at the onset of clumsiness of picking apples, but 1–3 weeks later could not flex the elbow joint and raise the forelimb, indicating the motor weakness had spread to the proximal muscles (Fig. 1D). In the late stage, 2–5 weeks after the onset, the dominant hand muscles became completely paralysed (Fig. 1A), and muscle weakness and atrophy had spread to the contralateral, un-injected side limb muscles (Fig. 1B and E). One of TDP-43-expressing monkeys showed respiratory failure at the end stage. The control monkeys did not show obvious motor symptoms, indicating surgical procedure or virus toxicity was minimal (Fig. 1C–E and Supplementary Video 2).

Electrophysiological findings

Electrophysiologically, in all TDP-43-expressing monkeys, the compound muscle action potential of the thenar muscle evoked by stimulation of the median nerve at the wrist progressively decreased in size with preservation of conduction velocity, and the muscle became unexcitable in the late stage (Fig. 2A). In contrast, three monkeys injected with control AAV did not show a marked change compound muscle action potential size (Fig. 2A). In TDP-43-expressing monkeys, the compound muscle action potential size on the contralateral side was not changed in the early stage (3–5 days after the onset of motor symptoms), but showed milder reduction of compound muscle action potential size in the late stage (Fig. 2B). Needle EMG revealed robust fasciculation potentials, and denervating potentials of positive sharp waves and fibrillation potentials in the late stage (Fig. 2C).

Cytoplasmic mislocalization with loss of endogenous monkey TDP-43, dystrophic neurites and cystatin C-positive granules in the cytoplasm

Neuropathologically, an anti-Flag antibody widely detected exogenous TDP-43 in neurons from the second cervical to the second thoracic segments on both sides, and was observed in almost all neurons on the injected side from the fourth to eighth cervical segments. Generally, Flag immunoreactivity was not detected in the glial cells. There was no inflammatory reaction except for in the area around the injection site. In the late stage, exogenous TDP-43 was observed in either the nucleus or cytoplasm (Fig. 3A). Pan-TDP-43 staining revealed that most motoneurons with cytoplasmic TDP-43 lost endogenous monkey TDP-43 staining (Fig. 3B), which normally localized in the nucleus (Fig. 3C). Mislocalized TDP-43 was diffusely distributed in the cytoplasm

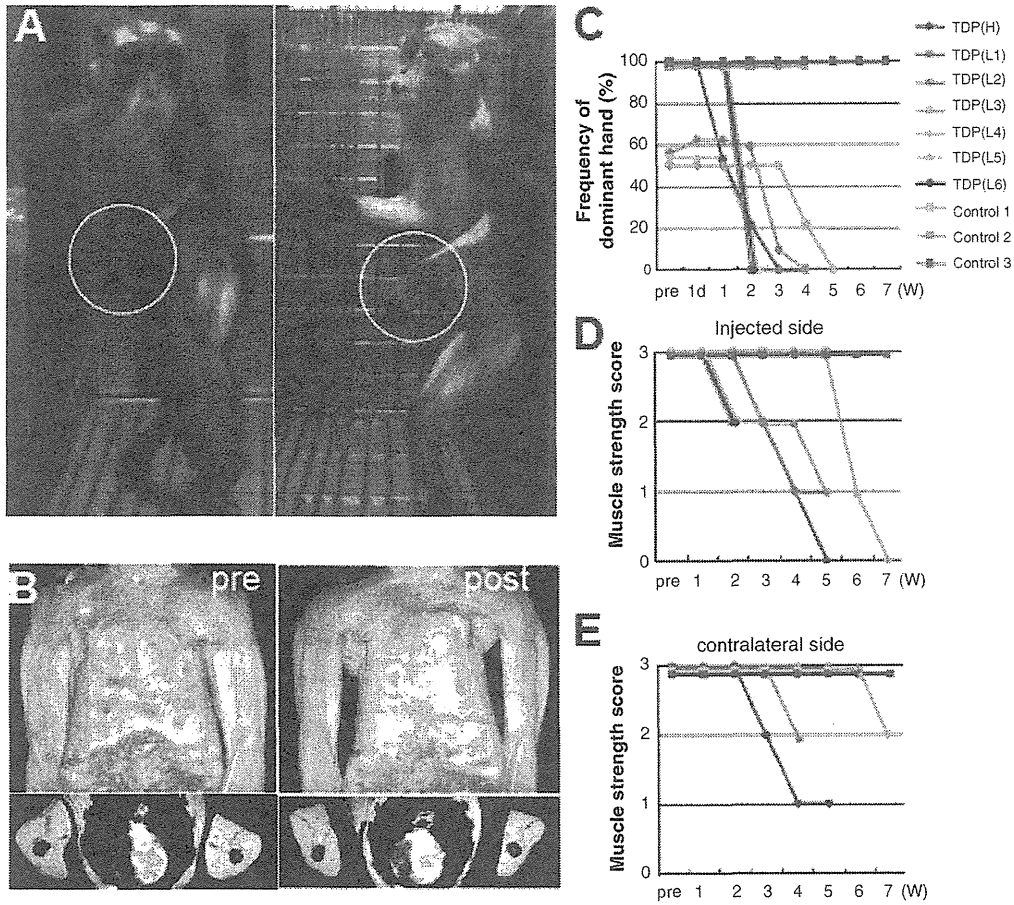

Figure 1 Overexpressing wild-type TDP-43 in the monkey cervical cord leads to progressive motor weakness and muscle atrophy. (**A**) Motor paresis of the forelimb on the injected side (encircled) in TDP-43 AAV-injected monkeys. (**B**) Constructed (*top*) and axial (*bottom*) MRI images of upper arm muscles before (pre) and 4 weeks after (post) injection, indicating a marked muscle atrophy of upper and forearms as well as hand muscles, predominantly on the injected side (left side). (**C**) Apple test. Frequency with which the dominant hand was used to pick up apples. (**D** and **E**) Behavioural analysis assessing muscle strength of forearms on the injected side (**D**) and contralateral side (**E**). A score of 3 indicates that the monkeys can hang on the ceiling fence; score of 2, they can grasp but not hang on the ceiling fence; score of 1, they can raise the forelimb but not reach ceiling fence; score of 0, they cannot raise the forelimb. Measurements that appear to end before the end of the experiment are from the three monkeys that were pathologically examined in the early stage.

and, in some neurons, granularly aggregated (Fig. 3B). Proximal and distal dystrophic neurites were occasionally observed (Fig. 3A and B). Phosphorylation of TDP-43 in the nucleus or cytoplasm was not clear in the early stage, but became obvious in the late stage (Fig. 3D). Anti-ubiquitin and anti-p62 antibodies did not show a clear abnormal signal. Astrogliosis and microgliosis were observed (Supplementary Fig. 3). A small fraction of the motoneurons expressing TDP-43 in the nucleus characteristically displayed coarse cystatin C-positive granules in the cytoplasm (Fig. 3E) in the neurons with exogenously expressed TDP-43 in the nucleus. There were no neurons with co-localized cystatin C-positive granules and TDP-43 aggregates in the cytoplasm. We also observed aberrant accumulation of phosphorylated neurofilaments (Fig. 3F) and peripherin (Supplementary Fig. 4) in the cytoplasm of spinal motoneurons, a common pathological feature in patients with ALS (Munoz *et al.*, 1988; Corbo and Hays, 1992). Immunostaining with an anti-Flag antibody identified its nuclear or cytoplasmic immunoreactivity in some Betz cells in the precentral gyrus restricted to the forelimb area contralateral to the injection. This Flag immunoreactivity was not observed in other cortical areas (including hippocampus and frontal lobe, which are preferentially affected in patients with FTLD), thalamus, basal ganglia and white matter, or in glial cells (Supplementary Fig. 5).

Characteristic regional mislocalization of TDP-43 in motoneurons of the anterior horn similar to amyotrophic lateral sclerosis spinal cords

In the early stage, 3–5 days after the onset of hand clumsiness, TDP-43 mislocalization of diffuse staining pattern was observed in

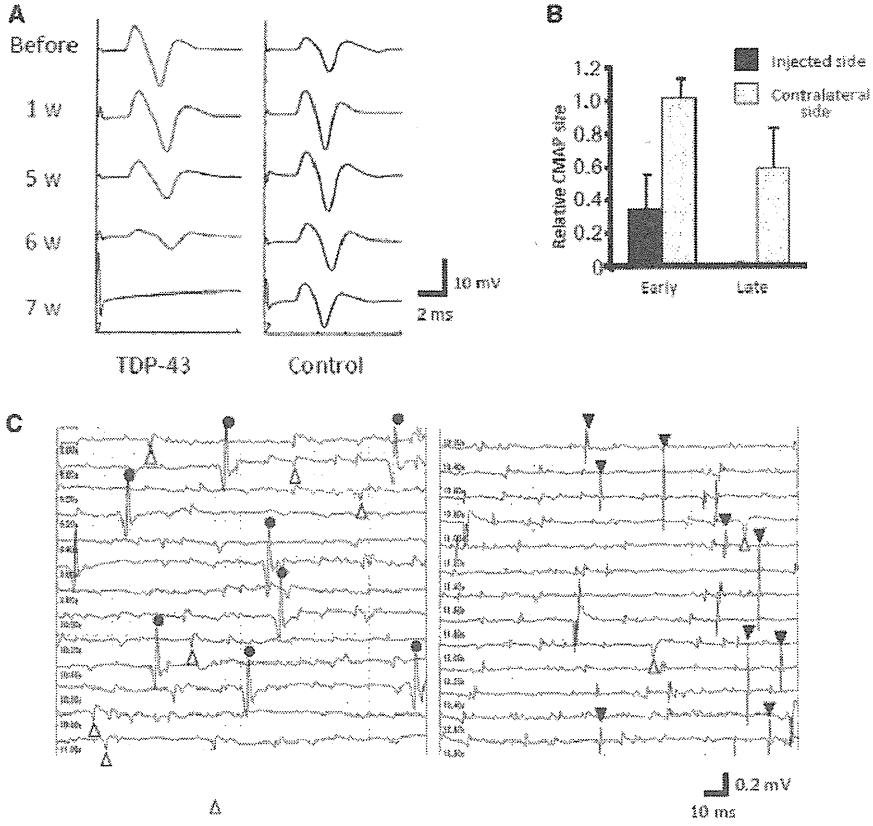

Figure 2 Electrophysiological findings for motor symptoms of the monkeys. (**A**) Compound muscle action potentials (CMAPs) in the thenar muscle after stimulation of the median nerve at the wrist. They gradually decreased in size, and became inexcitable in the late stage. There was no change of compound muscle action potential size in the control monkey. (**B**) Ratio of the compound muscle action potential size 3–5 days after the onset (early stage) or 2–5 weeks after the onset (late stage) to the size before injection. In the early stage, there was no reduction in compound muscle action potential size on the contralateral side, but moderately attenuated in the late stage. (**C**) Needle EMG findings of the forearm muscle. Circles indicate fasciculation potentials; open triangles, positive sharp waves; filled triangles, fibrillation potentials.

most motoneurons in the lateral nuclear group of the anterior horn. In contrast, almost all neurons in other areas of the spinal cord including the posterior horn showed flag signal of exogenously expressed TDP-43 only in the nucleus (Fig. 4A and D). Importantly, the contralateral lateral nuclear group also exhibited TDP-43 mislocalization on the side of forelimb that did not yet show obvious motor symptoms (Supplementary Fig. 6). Signals of exogenous Flag-TDP-43 were detected by real-time polymerase chain reaction on the contralateral half of the spinal cord (Supplementary Fig. 7). However, this distribution indicates that this regional selectivity is not due to differences in the concentration of the injected AAV, but rather is due to properties of the affected neurons. In the late stage, 2–5 weeks after onset, the percentage of motoneurons with TDP-43 mislocalization decreased ~47% in the lateral nuclear group, and was <2% in the ventromedial nuclear group (Figs 3B and 4D). The number of large motoneurons ($\geqslant$20 μm) in the early stage in this lateral nuclear group did not change, but in the late stage, was reduced by ~42% (Fig. 4B, C and E). In contrast, the reduction in the number of large neurons in the ventromedial nuclear group was not significant (control, 1.78 ± 0.20 versus TDP-43, 1.68 ± 0.18/section, $P = 0.80$). Astrogliosis was also more prominent in the lateral area than in the ventromedial area of the anterior horn (data not shown). Motoneuronal degeneration of the lateral nuclear group was also confirmed by studying the anterior roots of the eighth cervical segment, which showed frequent myelin ovoids and loss of large myelinated axons ($\geqslant$8 μm) in the late stage, although they were almost normal in the early stage (Fig. 5A–C). This axonal loss in the anterior roots is consistent with pathological change of the thenar muscle, showing numerous small angulated atrophic fibres (Fig. 5D).

We furthermore examined whether such a regional change of TDP-43 mislocalization occurs in spinal cord of nine patients with ALS with upper limb weakness and hand muscle atrophy. TDP-43 mislocalization was observed much more in the lateral nuclear group than in the ventromedial nuclear group of the cord at the eighth cervical segment (Fig. 6A–C).

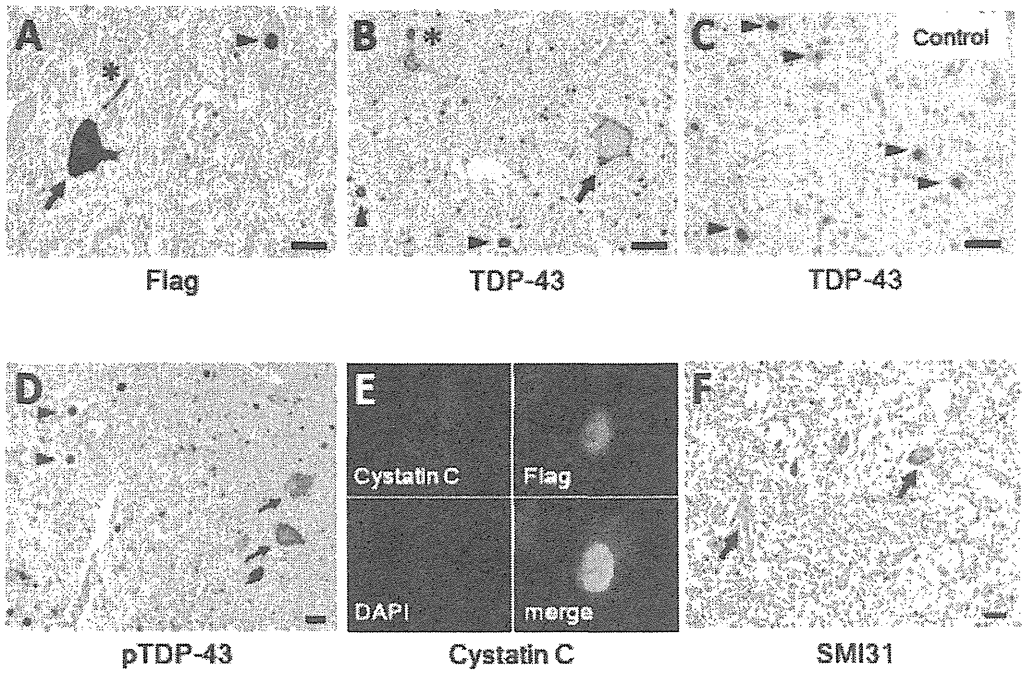

Figure 3 Neuropathological findings of monkey spinal cords of TDP-43–overexpressed monkeys at the late stage (**A**, **D–F**), and control with mock AAV (**C**). (**A–D**) TDP-43-overexpressed spinal cord immunostaining using antibodies to Flag (**A**), pan-TDP-43 (**B**) and pS409/410 TDP-43 (**D**) demonstrated mislocalization in cytoplasm (arrows), and dystrophic neurites (asterisks) as well as normal localization in nuclei (arrowheads), whereas normal spinal cord showed only nuclear localization of TDP-43. (**E**) Co-labelling of a motoneuron expressing TDP-43 in the nucleus with antibodies to cystatin C (red) and Flag (green). The nucleus is labelled with DAPI. (**F**) Immunostaining using SMI31 revealed the aberrant presence of phosphorylated neurofilament in the neuronal cytoplasm (arrows). Scale bars: 20 μm. Immunostainings of spinal cord with control mock AAV using the antibodies to Flag, pS409/410 TDP-43, cystatin C and SMI31 are shown in Supplementary Fig. 7.

Interspecies differences in TDP-43 pathology in rodents and primates

To investigate interspecies differences in TDP-43 pathology, we injected the identical TDP-43-expressing AAV at the same concentration into rat cervical cords. Expression level of Flag-TDP-43 messenger RNA around the injection site in rat spinal cord was >20-fold higher than that of endogenous TDP-43 level, and this fold change was similar to that in monkey spinal cord (Fig. 7A). Rats injected with TDP-43 AAV showed progressive motor weakness (Fig. 7B), measured by grip strength. Importantly, exogenous TDP-43 was observed only in the nuclei of motoneurons in both early (14 days after injection of AAV) and late (4 weeks after injection of AAV) stages (Fig. 7C). Since mislocalization of TDP-43 in the monkey spinal cords was more prominent in the early stage (14 days), we also examined the pathology of rat spinal cords at a very early stage (7 days); however, the weak Flag immunoreactivity was still limited to the nucleus of motoneurons (data not shown). Furthermore, this rat model failed to exhibit cystatin C-positive aggregates, dystrophic neurites, or aberrant accumulation of phosphorylated neurofilaments in the cytoplasm of spinal motoneurons (Fig. 7D). These neuropathological findings indicate that this rat model was less similar to human ALS than our monkey model in TDP-43 localization and other characteristic features of ALS.

Detection of the 25-kDa C-terminal fragment and phosphorylated TDP-43 in the early stage

Biochemically, immunoblot analysis of monkey spinal cord demonstrated that the exogenous Flag-tagged TDP-43 became much more insoluble than endogenous TDP-43 (Fig. 8A). The phosphorylation of TDP-43 was unclear in the early stage (Fig. 8B) but clearly detected later (Fig. 8C). Neither a C-terminal nor a phosphospecific TDP-43 antibody detected the 25-kDa C-terminal fragment (Fig. 8A–C). These suggest that neither phosphorylation of TDP-43 or its 25-kDa C-terminal fragment in spinal cord is necessary to initiate motoneuronal dysfunction and degeneration in our monkeys.

Discussion

Frequent mislocalization of TDP-43 in the cytoplasm and loss of its nuclear staining are major pathological hallmarks in the histological

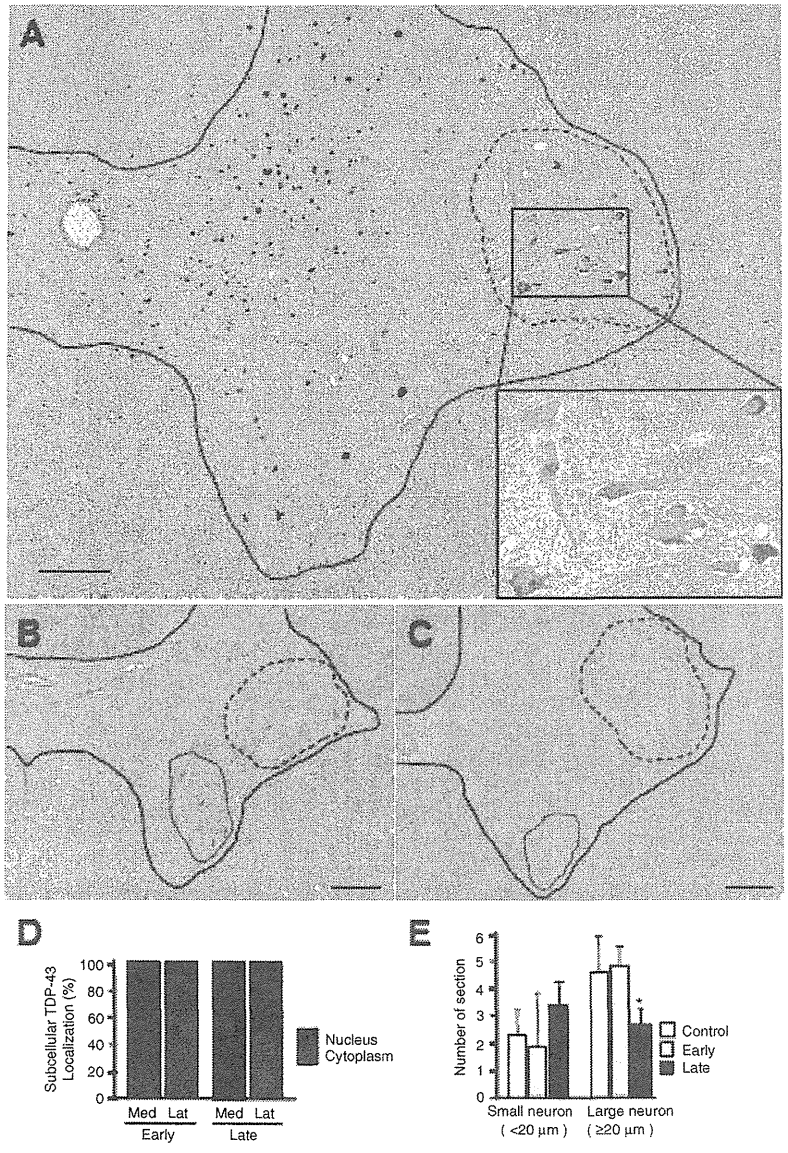

Figure 4 Regional mislocalization of TDP-43 and cell death in monkey spinal cords. (**A**) Sections from the injected side of the eighth cervical segment of the cord taken at the early stage and immunostained with an anti-Flag antibody. Most neurons in the lateral nuclear group (area encircled by broken line) showed cytoplasmic mislocalization of TDP-43 (inset), but almost all neurons in other areas expressed exogenous TDP-43 in the nucleus. Scale bars: 200 μm. (**B** and **C**) The eighth cervical level of cord from monkeys injected with TDP-43–expressing (**B**) and control (**C**) AAV, taken at the late stage and stained with haematoxylin and eosin. The number of large motoneurons decreased in the lateral nuclear group (areas encircled by broken line), but not in ventromedial nuclear group (areas encircled by red solid line). Scale bars: 200 μm. (**D**) Percentage of neurons with nuclear (black) or cytoplasmic (red) localization of exogenous TDP-43 in the lateral nuclear groups on the injected side. Neurodegeneration affects the lateral nuclear group more than the ventromedial nuclear group. (**E**) Cell count of neurons in the lateral nuclear group on haematoxylin and eosin staining. Mean ± SEM. $n = 3$, $^*P < 0.05$. Lat = lateral nuclear group; Med = ventromedial nuclear group.

diagnosis of ALS and FTLD (Geser *et al.*, 2010). The classification of TDP-43 proteinopathy is based on a combination of neuronal cytoplasmic inclusions and dystrophic neurites (Mackenzie *et al.*, 2011). The morphological features in our monkeys are close to type B TDP-43 proteinopathy, which is usually observed in the brains of patients with ALS. The only difference between the pathology of our monkeys and type B TDP-43 proteinopathy is that mislocalized cytoplasmic TDP-43 was usually diffuse and neuronal cytoplasmic inclusions were less frequent in our monkeys. Since this monkey is an acute model for TDP-43 pathology, it possibly

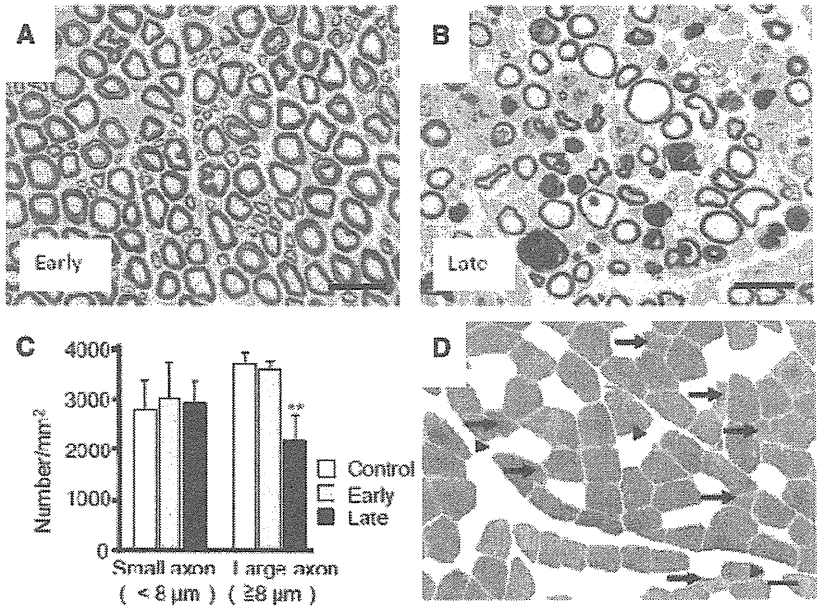

Figure 5 Pathological finding of monkey anterior root and skeletal muscle. Toluidine blue staining of the eighth cervical anterior roots on the injected side in the early (**A**) and late (**B**) stages, and their myelinated axon densities (**C**). Mean ± SEM, $n = 3$, $^{**}P < 0.01$. (**D**) Transverse section of the biceps brachii muscle from a TDP-43–expressing monkey 4 weeks after injection, stained with ATPase (pH 10.6). Small angulated atrophic changes of type I (arrowheads) and type II (arrows) fibres, with predominant involvement of type II fibres, can be seen. Scale bar: 50 μm.

takes more time for diffusely mislocalized TDP-43 to be aggregated. Moreover, in the spinal cords of patients with ALS, diffuse cytoplasmic TDP-43 staining is more common, and neuronal cytoplasmic inclusions are less frequent than in the brain and may even be absent (Giordana *et al.*, 2010). Thus, our monkey model shows the key features of TDP-43 proteinopathy as seen in the ALS spinal cord.

Interestingly, despite the diffuse expression of exogenous TDP-43 in the spinal cord, TDP-43 mislocalization and neuron loss predominantly occurred in the lateral nuclear group in Rexed lamina IX, in which large neurons are mostly α-motoneurons (Carpenter *et al.*, 1983). The sensory neurons and interneurons in laminae III–VIII rarely showed TDP-43 mislocalization, and large motoneurons in the ventromedial nuclear group, most of which are also α-motoneurons, showed much less TDP-43 mislocalization and neuron loss. Within lamina IX, the lateral nuclear group innervates the distal, fast-contracting muscles of the extremities, and the ventromedial nuclear group innervates the posture-related, continuously contracting muscles attached to the axial skeleton (Carpenter *et al.*, 1983). This regional vulnerability among α-motoneurons is consistent with the distal hand or foot muscles being the first involved in 73% of patients with non-bulbar ALS (Harverkamp *et al.*, 1995; Körner *et al.*, 2011) and might be related to axon length, which affects axonal transport (Bilsland *et al.*, 2010), or to the preferential susceptibility of fast-fatigue rather than slow motoneurons (Dengler *et al.*, 1990; Pun *et al.*, 2006). Furthermore, in nine patients with ALS, more TDP-43 mislocalization was observed in the lateral nuclear group than in the ventromedial nuclear group of the eighth cervical cord segments. Taking these results together, we think that the tropism of TDP-43 mislocalization was similar to that of ALS pathology. However, expression levels of exogenous wild-type TDP-43 in our monkey and rat models were very high (~20-fold higher than that of endogenous TDP-43), which was partly due to lack of 3′-untranslated region in our TDP-43 expression construct. This is probably because TDP-43 controls its own expression through a negative feedback loop by binding to 3′-untranslated region sequences in its own messenger RNA (Ayala *et al.*, 2010; Polymenidou *et al.*, 2010). The unphysiologically high level of TDP-43 expression in our animal models should be taken into consideration when interpreting our findings.

Since Flag TDP-43 messenger RNA was detected in the spinal cord contralateral to the injected side by real-time polymerase chain reaction analysis, the AAV virus was shown to spread contralaterally through the spinal cord causing motor paresis and reduction of compound muscle action potential size in the opposite forelimb. However, it is still possible that there was concomitant cell-to-cell or trans-synaptic propagation of Flag TDP-43 protein in the spinal cord. Moreover, it is interesting that the Flag-TDP-43 signal was selectively extended into Betz cells in the forelimb area of precentral gyrus contralateral to the injection side, which can be explained by a retrograde progression from α-motoneuron in the cervical cord. More sophisticated experimental paradigms are necessary to distinguish whether it is the AAV vector itself,